Lawrence Berkeley Laboratory
UNIVERSITY OF CALIFORNIA

To be published as a Chapter in Heavy Ion Science,
D.A. Bromley, ed., New York, NY, Plenum Press

POSITIVE HEAVY ION SOURCES

David J. Clark

January 1983

NUCLEAR SCIENCE DIVISION

Prepared for the U.S. Department of Energy under Contract DE-AC03-76SF00098

DISCLAIMER

LBL-15543

Positive Heavy Ion Sources*

David J. Clark

Lawrence Berkeley Laboratory
University of California
Berkeley, CA 94720

January 1983

*This work was supported by the Director, U. S. Office of Energy Research, Division of Nuclear Physics of the Office of High Energy and Nuclear Physics, and by Nuclear Sciences of the Basic Energy Sciences Program of the U. S. Department of Energy under Contract No. DE-AC03-76SF00098.

Table of Contents

1. INTRODUCTION

Ion sources were developed soon after the discovery of ions in gas discharges in the late 1800's (Va 77). The initial uses were for mass spectrometry and for nuclear physics accelerators. In recent years, more versatile accelerator sources have been required to meet the need for a broad range of ion species, intensities, duty factors and to fit the geometric requirements of various accelerator types. Positive heavy ion sources are used in accelerators such as dc types, cyclotrons and linear accelerators. The resulting beams are used for the many fields of research described in these volumes, including nuclear and atomic science, ion implantation, radiography and therapy, and fusion power. There is generally a premium placed on producing beams with the highest possible charge state in an accelerator source, because the higher charge state allows a lower voltage dc accelerator or shorter linac to provide a given energy, since energy is charge times total voltage gain. For a cyclotron, energy is proportional to the square of the charge, giving an even higher incentive to get high charge states from the source. In this chapter, "heavy" ions will mean those heavier than helium. This chapter will emphasize the positive heavy ion sources used for the above fields. For other types of sources other references are available. Ion implantation sources are described in a book by Dearnaley et al. (De 73), and in a series of conferences. Isotope

separator sources are discussed in a series of conference proceedings, the most recent of which is (Am 76). Previous reviews of positive ion sources and their beams include those by Thonemann (Th 53), Vorob'ev and Pasyuk (Vo 70), Bennett (Be 71), Eninger (En 71), Septier (Se 72), Winter and Wolf (Wi 74), Green (Gr 74), Arianer (Ar 75), Clark (Cl 77), and Sidenius (Si 78).

2. PRODUCTION OF IONS

To create singly or multiply charged positive ions we must remove one or more electrons from an atom or ion, which requires energy. This energy can be supplied by a bombarding electron, by a heated surface of high work function, by a very high electric field or by a photon. In this section, we will describe two of the above processes which are of greatest importance in the ion sources of this chapter: electron bombardment and surface ionization.

2.1. Electron Bombardment

The most common method of producing ions is by bombarding atoms or molecules with electron beams of energy greater than their ionization potential. The range of ionization potentials involved in the wide variety of heavy ion elements and charge states is illustrated in Fig. 1. The "total ionization potential" shown in this figure is the sum of all the ionization potentials between the neutral atom state and the charge state shown on the contour lines. For example, the total ionization potential for $^{84}Kr^{11+}$ is

about 1300 volts, and the additional ionization potential to go to $^{84}Kr^{12+}$ is about 400 volts. The energy to remove the last electron from ^{84}Kr is 17 keV, and from ^{238}U is 129 keV (Ca 70). The total ionization potential is an approximate measure of the difficulty of producing the ion in a source.

The cross-section for ionization from one charge state to the next is a function of the ionization potential and the electron bombarding energy. The variation of cross-section with energy for ionization from neutral atom or molecule to charge state 1^+ is shown in Fig. 2 for several gases. It starts at zero at the ionization potential, reaches a maximum at an electron energy of about three times the ionization potential, and then falls with increasing electron energy.

To make calculations on the ionization process, it is convenient to fit these ionization cross-sections with an empirical formula. A formula used frequently is that of Lotz (Lo 68):

$$\sigma_{i\rightarrow i+1} = \sum_{j=1}^{N} a_j q_j (E_e V_j)^{-1} \ln (E_e/V_j) \qquad (1)$$

for $E_e >> V_j$, where j is the subshell number, q_j is the number of electrons in the j subshell, N is the number of subshells, E_e is electron energy, V_j is ionization potential of electrons in the j subshell, and a_j is the fitting parameter. The summation is taken over all the remaining subshells of the ion. Lotz showed that equation (1) provided a good fit

to measured cross-sections for low charge states.

The equations for the time evolution of the charge states can be written as a set of differential equations:

$$\frac{dn_q}{dt} = jn_{q-1}\,\sigma_{q-1\to q} - jn_q\sigma_{q\to q+1} \qquad (2)$$

where n_q is the density of ions of charge state q (ions cm^{-3}), and j is the electron beam density (electrons $cm^{-2}\,s^{-1}$). If this set of equations is integrated, using the Lotz cross sections with a fixed E_e, we get, for example, the time evolution plot for argon shown in Fig. 3, as calculated by the Orsay group for 10 keV electrons. This assumes no charge exchange with background gas or recombination with electrons. The ionization factor, $j\tau$, of Fig. 3, is a convenient figure of merit of the source, which determines the average charge state expected. This can be seen also from the relation that the rate of ionization of a single ion is $j\sigma_{i-1\to i}$. The time for this transition is then $(j\sigma_{i-1\to i})^{-1}$, and the total time for ionization from neutral atom to charge state i is

$$\tau = \sum_{i=1}^{i} (j\sigma_{i-1\to i})^{-1} \quad \text{or}$$

$$j\tau = \sum_{i=1}^{i} (\sigma_{i-1\to i})^{-1} \qquad (3)$$

This equation separates the variables into the source properties on the left and the atomic cross-sections on the right. To produce any desired charge state of an ion, we need to bombard it with an electron beam flux density j for a time τ to obtain the desired product $j\tau$ (electrons cm^{-2})

or (coulombs cm^{-2}). Confinement sources such as the EBIS can have confinement times up to several seconds, as we shall see. Short pulse sources such as the laser have submicrosecond pulse length. In all sources, higher j values are valuable to produce higher charge states in a given time, or to produce a given charge state in a shorter time to allow higher source repetition rate. The Orsay group has calculated the right hand side of equation (3), using the Lotz cross-sections, for the many ion species and charge states required, and plotted them as shown in Fig. 4. This comprehensive figure shows the $j\tau$ necessary over a wide range of desired ions. Shown on the right hand scale is the product $n\tau = j\tau/(ev)$ where e is electron charge and v is electron velocity. $n\tau$ is a familiar quantity used as a criterion for plasma confinement in fusion reactors. However, a fusion reactor requires high ion temperature while ion sources require high electron temperature, which is easier to obtain. The ranges of $n\tau$ and electron energy in several high charge state ion sources are shown in Fig. 5. The operating range of the most widely used high charge state source, the PIG, is shown on the figure. The advanced sources have higher values of $n\tau$ and E_e, opening up a region of higher charge states.

Figure 6 presents a survey of charge states available for all the elements for various ion sources, fusion plasma machines, and beams stripped by sending beams from accelerators such as the SuperHILAC or Bevalac through foils or

gases. Since the time this figure was assembled in 1977, EBIS sources have increased their Q values to the range of the SuperHILAC, and ECR sources have improved somewhat. An ion source is, of course, a much cheaper device for producing high charge states than these large accelerator systems, but the accelerators have higher intensities.

2.2. Stripping of Fast Ions

We have examined in Section 2.1 the usual method for producing ions of both low and high charge state: bombardment with fast electrons. What is required is a high relative velocity between the electrons and the atom or ion. So another method for producing high charge state ions is by accelerating low charge state ions, and then sending them through a stripping foil or gas to get a higher charge state using the bombardment of the electrons in the stripper atoms for ionization. It is easy to get sufficient $n\tau$ to reach the "equilibrium thickness" of stripper at which the probabilities of electron loss and pickup are equal. The difficulty is in accelerating the ion to high enough velocity to get a high equivalent E_e. Stripping cross-sections and charge state distributions were reviewed by Betz (Be 72). Stripping systems are used by the large heavy ion accelerators, where the highest charge state produced by the ion source (in adequate intensity) is accelerated by the first stage, the beam is stripped to a higher charge state, and then it is accelerated by the second stage. A much higher energy can thus be reached by the second stage by using

stripping. Examples of this two-stage system are the "pre-stripper" and "post-stripper" sections of heavy ion linacs such as the Berkeley SuperHILAC and Darmstadt UNILAC, stripping between the tandem accelerator and the cyclotron at Oak Ridge, and stripping planned between cyclotrons at Michigan State University and at GANIL in France. The charge states available by stripping the full energy beams of several heavy ion accelerators are shown in Fig. 6. These types of ions are useful for atomic physics studies.

In comparing the methods of ionization by fast ion stripping with that of electron bombardment, we can see that fast ion stripping requires much more expensive equipment. For example, an ion of mass 100 with the same velocity as a 1 keV electron has an energy of about 2 MeV/nucleon, which requires an accelerating voltage of 20 MV for a typical charge/mass of 0.1 from an ion source. This takes an expensive accelerator. But until higher charge state ion sources are available, this two-stage design is the best way to generate high energy heavy ion beams.

2.3. Surface Ionization

Surface ionization (or contact ionization) is a process in which an atom hits a heated surface and emerges from the surface as an ion. It occurs most efficiently when an atom or molecule with a low ionization potential impinges on a heated surface of a material with a high work function (Va 77). This phenomenon was discovered in the early 1920's

by observing the ionization of cesium on a hot tungsten surface. The ion current density as a function of surface temperature is shown in Fig. 7. Atoms with low ionization potentials include cesium (3.9 eV), potassium (4.3 eV), and rubidium (4.2 eV). Some high work function materials which are useful for the hot surface are tungsten (4.5 eV), platinum (5.3 eV), and iridium (5.3 eV). An example of a large cesium source will be given later in this chapter.

3. BEAM EXTRACTION, FOCUSING, AND DIAGNOSTICS

After positive ion production in the source, we must form a beam with an extraction system. The subject of beam formation has been reviewed by Green (Gr 74, Gr 76). The extractor normally takes the form of an electrode biased negative relative to the source, and having an aperture through which the beam passes. Examples are shown in Figures 16, 19, 20, 28, 34, and 40 for various types of sources. The source aperture is often indented in a conical shape as in Figures 15 and 18 to produce a converging electric field to counteract the diverging space charge forces of high intensity beams. The extractor often has a matching shape, as in Fig. 20, to reinforce this converging electric field. This shape is sometimes called "Pierce geometry", in analogy to electron gun design by John Pierce. In practice, the source is usually biased to positive potential and the extractor grounded, to provide a beam at ground potential.

Since the beam is usually diverging when exiting the ion source and extractor system, lenses are used to focus and transport it to the target or accelerator system. These are often electrostatic cylindrical lenses such as einzel lenses, as shown in Figures 28 and 34. Bending magnets can also be used as focusing elements, as in the source magnet of Fig. 11. Other frequently used lense types are magnetic solenoids and electrostatic quadrupoles for low energy beams, and magnetic

quadrupoles for higher energy beams.

After the beam is formed and focused, it is important to measure its most important characteristics: ion species and intensity, emittance, energy spread, and time structure. The ion species is usually measured by a magnetic analyzer, which separates ions by charge/mass ratio. To determine the mass, other checks must be made such as shutting off the gas feed to watch for disappearance of the beam, looking for isotopes in the expected abundance, and observing the other charge states produced. For species with almost identical masses, such as ^{14}C and ^{14}N, the beam can be accelerated to several MeV and separated by differential energy loss or range. In multi-charged heavy ion work, one must be always alert to the possibility of mis-identification because of the many similar charge/mass ratios possible with various impurities, isotopes, and charge states. There have been many cases of the wrong beam being delivered to an accelerator target due to this problem (even with relative light ions such as H_2^+, $^2H^+$ and He^{2+}).

An important characteristic of a beam is that of emittance. Emittance is the area of the beam in "transverse phase space" (displacement and divergence in a direction transverse to the beam direction). A comprehensive description of beam emittance is given by Banford (Ba 66). A briefer summary is given for example by Clark (Cl 72). A measure of emittance is the width times the divergence at a waist or focus. The units of emittance are mm mrad or m rad, for example. The quantity ε_n, "normali-

zed emittance", is often used: $\varepsilon_n = \beta\gamma\varepsilon$, where ε is the "un-normalized emittance" as described above, $\beta = v/c$, c is the speed of light, $\gamma = (1-\beta^2)^{-\frac{1}{2}}$. ε_n has the same units as ε. Some labs use $\varepsilon_n = \varepsilon E^{\frac{1}{2}}$, in which case the units might be mm·mrad $(MeV)^{\frac{1}{2}}$. Normalized emittance is a useful concept because it should remain constant as the beam accelerates, if no aberrations occur. The un-normalized emittance, ε, should decrease with acceleration because the acceleration increases the longitudinal velocity component while leaving the transverse velocity fixed, thus reducing the beam divergence. Each beam transport system and accelerator which the ion source feeds has an "acceptance", which is the maximum emittance that it can accept. So, it is important to measure the emittance of an ion source to determine how much of it will fit into the acceptance of the later stages of the system. The ratio of the beam current to the product of the emittances in the two directions transverse to the direction of travel is the beam brightness. It is a useful quantity for comparing one source with another. Its units might be A sr^{-1} cm^{-2}. One also needs to know the beam current, for complete evaluation of a source.

Some systems for measurement of emittance will be described here. In Fig. 8 is shown an automatic emittance measuring system used for negative ion beams at Oxford University. The incoming beam at the left is defined by a slit, which is moved to the edge of the beam to start. The magnetic

deflector sweeps the beam across the Faraday cup at the right and the current vs. time is recorded on a multichannel analyzer. The stepping motor moves the slit into the beam to the next position and another deflector sweep takes place. This program is repeated until the slit has moved completely across the beam. Each deflector sweep cycle takes 10 s and the whole measurement takes seven minutes. The data is processed by a PDP-10 computer and the resulting phase space area plotted with brightness contours as in Fig. 9. Other output available includes the raw data from the multichannel analyzer, and a plot of brightness versus emittance area. In Fig. 10 is shown an example of a beam with aberrations, whose origin is believed to be the non-linear electric fields at the extraction gap. Several other laboratories have automatic emittance gear such as this. It provides an excellent record of source operation.

In Fig. 11, we see an example of a simpler emittance measuring system that was used at Lawrence Berkeley Laboratory. It consists of plates with slots or rows of holes which break the beam up into beamlets. Downstream from the plate is an X-Y scan on a storage oscilloscope. The scan wire sweep speed is typically 2 Hz, allowing convenient tuning of the source parameters to optimize the brightness. The oscilloscope readout is shown at the bottom of Fig. 12. The top of Fig. 12 shows the calculated emittance area plots from this data. The accuracy is not as high and the data processing

is not automatic as at Oxford, but tuning is much faster.

Another important characteristic of an ion beam is its energy spread. A nice example of a system to measure energy spread is shown in Fig. 13. This is an Oxford University system with potentials arranged for a negative ion beam, but the same system would measure a positive ion beam, with reversed voltage polarities. In this retarding field analyzer the beam is slowed down to approximately zero energy with a fine bias control on the retarding voltage. Beams of higher voltage than the extraction plus bias power supplies are transmitted through the small defining aperture in the plate between the retarding electrodes. Beams of lower voltage are reflected. So, the beam in the Faraday cup as a function of the bias supply voltage gives the integral energy spectrum. When this spectrum is differentiated, it yields data such as shown in Fig. 14. Here three negative ion sources are compared, showing energy spreads of 7-8 eV full width half maximum. This system is designed to be insensitive to small variations in extractor voltage, since both accelerating and retarding fields use the same power supply. In practice, one needs a supply capable of 10^{-4} regulation at 20 kV to prevent increase of energy spread. Keeping the energy spread low is important because transverse energy spread contributes to beam emittance. Also, low energy bunching is limited by beam energy spread.

The time structure is important in matching the require-

ments of the later stages of the system. For example, dc electrostatic accelerators and modern sector cyclotrons can accept dc beams. Heavy ion linacs usually run at 10-20% duty factor to minimize radio frequency power and hardward costs, and so require only this duty factor from the source, easing the problems of source power handling and lifetime. A heavy ion synchrotron has an even shorter duty factor of about .1%, further relaxing source requirements. Of course beam pulsing may be required for certain experiments, and can be done with a fast deflection and bunching system. Source noise can be a difficulty to some experiments, and is usually caused by plasma oscillations in source arcs operating at high power densities, particularly in magnetic fields. A compromise tuning must be reached to produce low noise and high output.

4. SOURCE DESCRIPTIONS

4.1. Low Charge State Sources

The low charge state sources discussed here will be limited to some recent examples of sources developed for high intensity heavy ion driven fusion applications, and a liquid metal source which is interesting for its extremely high brightness and micro-beam capability. Many other types of low charge state sources have been developed over the years and are well described in other references: the historical development of ion sources in (Va 77), isotope production sources in a series of conferences such as (Am 76), and ion implantation sources in

(De 73).

A heavy ion fusion reactor (see volume 3) requires either a "conventional" source injecting a conventional linac, or a high current source injecting an induction linac. The conventional source must supply a beam of about 50 mA of singly charged ions of mass 100-200 AMU, with a 1 ms pulse width and 1-10 Hz repetition rate. This requirement implies a scaling up of conventional low charge state sources such as a PIG or diode type source. The high current (1-10 A), shorter pulse (5 μs), type of source uses a large area surface ionization anode. It must supply the same number of particles/pulse as the lower current sources mentioned above for eventual bombardment of a pellet, after acceleration and bunching.

Figure 15 shows a Xe^{1+} source for heavy ion fusion developed by Hughes Research Laboratories as a scaled up version of a 2 mA Xe^{1+} ion implantation source. This is a PIG source (see Sec. 4.2.1.) with the arc operating at 50 V and up to 1A, and a low magnetic field of 50 gauss. It produced 30 mA of Xe^{1+} with 100 kV on the extractor gap, 1 ms pulse length with 0.2 - 1.0 Hz repetition rate. A stable plasma was maintained on the relatively large 3 cm diameter source aperture. It was installed on a 1.5 MV dc accelerator at Argonne National Laboratory, where it ran successfully.

The source shown in Fig. 16 was also developed for heavy ion fusion applications. It was adapted from an early small

scale version of a Berkeley multi-ampere magnetic fusion hydrogen injector. It is basically a diode source with eight tungsten filaments and a hemispherical anode. The absence of a magnetic field promotes noise-free arc operation. The source is pulsed at 0.5 ms length, at about 1 Hz. The arc supply provides up to 50 A at 300 V. The extractor used on this source is of the multi-aperture type, using 13 holes. This is a feature developed by the magnetic fusion source groups to obtain very large beam currents by expanding the number of extractor holes or slits over a large source plasma area. Another feature adapted from the magnetic fusion sources is the use of "accel-decel" geometry of the extractor. This system uses two gaps in series, the first to give the main acceleration and the second to give a small deceleration. The function of the second gap is to reflect electrons back toward the downstream beam area so that they neutralize the beam space charge effectively. For example, to transport the 30 mA, 20 keV beam from this source 1 m to a Faraday cup, it must be at least 97% neutralized. The normalized emittance was measured as $\varepsilon_n = .03\pi$ cm mrad, which is adequate for transport. The source was also installed in a 500 kV terminal and accelerated to ground, with 35 mA intensity.

The source in Fig. 17 was developed at GSI, Darmstadt for application to heavy ion fusion, and UNILAC heavy ion linac injection. It uses a PIG type structure, like the source of Fig. 15, but with the addition of 12 lines of permanent magnets with alternating

polarity in the anode, called a "picket fence". This is a feature used in a Culham, U.K. source to prevent plasma loss at the walls and thus increase efficiency. As seen in the figure, the extraction system is a multi-aperture (7 holes) accel-decel design like that of Fig. 16. This source has produced 30-50 mA of Xe^{1+}, with ε_n = 0.15 mm mrad. A number of gases from helium to xenon have been used, with intensity following the expected $(mass)^{-\frac{1}{2}}$ law.

The next source, Fig. 18, is also for heavy ion fusion, but for high current, short pulse operation. This is the Berkeley Cs^{1+} surface ionization source intended for induction linac injection. The advantages of a surface ionization source are the well-defined flat extraction surface (compared to a plasma) giving excellent emittance, and low impurity singly ionized beams. This source has a 30 cm diameter anode designed for 1A of current at 500 kV of extractor voltage with 4μs pulse length. Neutral cesium atoms are sprayed onto the hot ($1200^{o}K$-$1400^{o}K$) iridium anode. The output current followed the expected space-charge limited $V^{3/2}$ Childs law behavior up to 1 A at 500 kV. The emittance is measured as $\varepsilon_n = 2\pi$ mm mrad, better than required for further acceleration.

The last subject of this section is field ionization sources. These were described by Broers (Br 79). The source shown in Fig. 19 is a liquid metal field ionization source. This version was developed by Hughes Research Laboratories for ion microscopy

and microcircuit fabrication. The source is based on one developed by Clampitt et al (Cl 75). The requirements for maskless doping of semiconductors is a 5000 Å diameter spot, with >1 A cm^{-2} current. Ion sputtering can also be done with this source. The source operates by electric field emission from a small plasma ball of liquid gallium at the end of a sharp tungsten needle. The resulting beam has extremely high brightness of 3 x 10^6A cm^{-2} sr^{-1}. We can compare this to the brightness of a normal bright source, the duoplasmatron, of 200 A cm^{-2} sr^{-1} (Br 79). The current density is 1.5 A cm^{-2} in a 1000 Å diameter spot, at 59 kV. Grooves were machined with the 1000 Å beam in a gold film to successfully demonstrate the beam sputtering capability.

Another field ionization source of very high brightness is that of Orloff and Swanson (Or 75). It used H_2 gas ionized at the tip of an iridium needle with radius in the range 800-1500 Å. The pressure near the needle was 10^{-3} - 10^{-2} torr. The resulting beam had a brightness of >10^8 A $cm^{-2}sr^{-1}$, with current in the 10^{-10} A range. The size of the virtual source was estimated to be 10 Å. With further development these sources may be applied to ion beam micromachining, ion implantation, and ion microscopy.

4.2. Present High Charge State Sources

This section will discuss the two principle kinds of high charge state sources which are used on present day heavy ion accelerators, PIG sources, and duoplasmatrons. The advanced high charge state sources such as the EBIS and ECR source, which are in a few cases in routine operation, are mostly scheduled for future installation on accelerators, and will be discussed in Section 4.3.

4.2.1. PIG Sources

There were previous review papers on PIG sources by Bennett (Be 72b) and Green (Gr 74b). The PIG (Penning or Philips Ionization Gauge) source is the principal source used on operating heavy ion linacs and cyclotrons. It was used as a vacuum gauge by Penning in 1937 (Pe 37) and soon afterward sold by the Philips Company for that purpose.

The geometry and operation of a PIG source are shown in Fig. 20. In this simplest version, the cathodes start cold. An arc is struck by raising the arc voltage to about 3 kV and increasing the gas pressure. Background ionization starts the discharge. The arc current builds up as the cathodes heat to give thermionic emission, and is stabilized by the arc supply current regulator or ballast series resistor. The uniform magnetic field performs the valuable function of collimating the arc, so that each electron emitted by the cathode, or created by an ionization event, is constrained to move along a

field line, giving it a long path for further ionization. The electrons reflected by the cathodes oscillate up and down along the magnetic field lines, providing a high electron current density j, to create high charge states. The confinement time is just the drift time of the ion from formation to extraction, the order of microseconds. Gas can be fed in at the cathode or anode. For a side extraction source shown here, a slot is cut in the side of the anode to allow an extractor electrode with a similar slot to pull ions out of the source. Some sources have end extraction through a hole in one cathode, but the charge states are usually lower in this case. Typically, the arc runs at 1-20 A and 300-2000 V. The source-extractor voltage is 10-30 kV, with the source usually being biased positive to give a beam at ground potential. The source can run dc or pulsed. Typical currents from accelerator PIG sources are shown in Table 1. The charge states shown are the highest having enough current for typical accelerator experiments.

There are several modifications of the basic PIG source of Fig. 20 which have been implemented in several laboratories. Some of these are shown in Fig. 21, the Dubna cyclotron PIG source of Pasyuk and Tretyakov. One feature of interest is the use of filament heating of one cathode (tungsten) by electron bombardment. The other cathode or "anticathode" (molybdenum) is well cooled. This system allows additional control over the arc impedance by adjustment of the bombardment

power. Another feature of interest is the insulated electrode half way up the anode. It is biased by an adjustable negative potential which causes sputtering of its atoms into the arc by the arc ions. This serves as an effective feed system for solid materials into the arc. The feed of solid materials may be up to 5 times less efficient than gas feed for beam production, depending on the feed system. This source is one of the most powerful of the accelerator PIG sources. It is typically pulsed at 30% duty factor.

The UNILAC group has adapted the Dubna source to service in a heavy ion linac injector. It is shown in Fig. 22. We see the filament heated hot cathode, the well-cooled anticathode, and the negatively biased sputter electrode in the anode for solid material feed. This source, located in a high voltage terminal, supplies the UNILAC with all required ion species up to U^{10+}. It is pulsed at 25% duty factor, to match the accelerator, which gives it a typical lifetime of one day.

In Fig. 23, we see the compact PIG source developed by Gavin for the pressurized super HILAC injector at Berkeley. It uses fairly cool titanium cathodes with a 20% arc duty factor. Two types of sputter electrodes are used, a standard central semi-cylinder in the top view, and a split ring electrode shown below. Increased currents of high charge states such as $Au^{9+,10+}$ are obtained with the ring electrode version. This source produces rather high charge states for such a small size, by careful optimization of geometry, cathode material and arc conditions.

Another example of a cyclotron PIG source is that of the LBL 88-inch Cyclotron, a sector-focused variable energy machine. Its internal source is shown in Fig. 24. The source uses some features of the ORIC cyclotron source of Oak Ridge. The arc-heated tantalum cathodes run hot. The arc is dc to match the cyclotron duty factor, but can be pulsed if required. A back insert block provides a solid material feed system by arc heating and back-bombardment (see Fig. 25). This insert is not biased electrically, so this system is not as versatile as that of Dubna, where more space is available inside the large first orbit of its classical cyclotron. Heavy ions from Li^{3+} to Ar^{8+} are generated with this source for nuclear science experiments.

Figure 25 shows a system of solid material feed developed by the Oak Ridge ORIC cyclotron group. It is based on the orbit trajectories of heavy ions in the source-extractor gap. The source is at ground potential and the "accelerating electrode" or extractor is attached to the dee, which has up to 80 kV of rf voltage at 10-20 MHz. The Oak Ridge group noticed an erosion at the back of their anodes in the position shown, and upon orbit analysis found that it was due to low charge state ions such as $Xe^{1+,2+,3+}$ being accelerated part way across the extraction gap, losing phase and accelerating back into the anode slit. They sputter atoms from the anode wall into the arc, where they are ionized and can be extracted and accelerated.

This was first observed as a copper beam, coming from anode material. This phenomenon was adapted to useful solid feed system by inserting blocks of the desired feed material.

PIG development is continuing in several laboratories to optimize the performance for required ion species, charge states, and accelerator geometry. The Dubna, Oak Ridge and Orsay cyclotron groups have done important development work. Development work is continuing at Berkeley on a PIG source producing ions such as Xe^{3+} and U^{5+} for the new SuperHILAC injector (Ga 81). Work is also underway at the GANIL laboratory on an injector PIG source for the coupled cyclotron system (Be 80).

4.2.2. Duoplasmatron Sources

The duoplasmatron is the traditional high brightness proton source for linac-synchrotron accelerator systems. It has been developed extensively at low duty factor for that purpose, and also in some laboratories for heavier ions. The most thorough development over the past decade has been done by GSI for the UNILAC heavy ion linac. The version of 1975 is shown in Fig. 26. The way this source operates is as follows. The filament electrons are accelerated toward the more positive polarity of the intermediate electrode and anode, forming an arc. The arc is concentrated in the intermediate electrode-anode region by the magnetic circuit excited by the magnet coil. A small hole in the anode allows plasma to diffuse into a plasma cup and be extracted by an extractor electrode (not shown). The particular features of high charge state heavy ion plasmas (electrode sputtering, high arc voltage) and a high duty factor

accelerator, required extensive design effort to obtain an effective source. An example of the electrode optimization studies is shown in Fig. 27. This shows how the redesign of the magnetic part of the electrodes moved the peak magnetic field point and highest plasma density into the anode hole region where extraction takes place. Also, a smaller hole in the intermediate electrode and a better cooled anode insert improved the high charge state output. Recently, (Ke 79) this source has been further improved by the addition of a larger expansion cup and a new cathode design to give currents of Ne^{1+} and Ar^{1+} in the 5-10 mA range. However, the better high charge state performance of the PIG has made it the operational source for the UNILAC.

4.3. Advanced High Charge State Sources

Over the past decade many ideas have been proposed for new higher charge state sources, to obtain the great savings in accelerator cost mentioned previously. These have included the HIPAC magnetic toroid device (Da 68) where 10 keV electrons would ionize and trap ions up to U^{60+} in several seconds. Work on this device has terminated. Another system was the electron ring accelerator (ERA) where fast electrons were injected into and trapped in a cyclotron-like magnetic field. The ERA was reviewed by Laslett (La 73). A study at Lawrence Berkeley Laboratory (La 74) estimated that Xe^{50+} would be the mean charge state in a high vacuum ring of

4×10^{12} electrons after one second. This proposal was not funded. In the plasma of magnetic fusion machines such as Tokamaks, very high charge state ions have been seen as impurities, as shown in Fig. 6, but a method of extraction is needed and the plasma volume is much larger than necessary for an ion source. In this section we will discuss two advanced sources which are being developed and installed on present accelerators, and which show promise of improved performance in the future. These sources are the Electron Cyclotron Resonance (ECR) source and the Electron Beam Ion Source (EBIS). They were reviewed by Loiseaux (Lo 81).

4.3.1. The Electron Cyclotron Resonance (ECR) Source

The ECR source uses a microwave generator to accelerate electrons at their cyclotron resonance frequency, ω_{ce}, in a magnetic field, B, where $\omega_{ce} = Be/m$. The electron charge/mass is e/m. At a field of 3.5 kG, the microwave frequency is 10 GHz. This type of source has been studied at several labs, including Oak Ridge, but has reached its highest development in Geller's group at the CEN lab at Grenoble, France.

The layout of Geller's large high charge state source, Super MAFIOS-B, is shown in Fig. 28. The operation of the source is as follows. Plasma of the desired species is produced in the small first stage by feeding in gas and microwave power. The microwave frequency, 16GHz, is equal to the electron cyclotron frequency at 6 kG. The component of the

microwave electric field perpendicular to the magnetic field accelerates the electrons, just as the electric field from the dee in a cyclotron accelerates ions, except that the frequencies are some thousand times higher, since the electron mass is 1800 times less than that of a proton. A few accelerated electrons produce more electrons by ionization, and a plasma is formed. The pressure in this first stage is 10^{-3} torr, a typical value for many ion sources. The charge state at this point is approximately the same as in a PIG source: 2^{+}-3^{+} for mass 10-20. An axial magnetic field of 6 kG guides the plasma to the second stage. Here the stripping to high charge states is done by the energetic electrons of up to 20 keV created by a second microwave resonance at 8 GHz corresponding to the magnetic field of 3 kG in the second stage. The background pressure in this second stage must be low to prevent charge exchange by the high charge state ions that are created. The pressure in SuperMAFIOS-B is 10^{-7} torr. For a long confinement time of the ions against plasma instabilities, a sextupole magnetic field is superimposed on the basic mirror configuration of the second stage, in a minimum B configuration. Geller, in fact, observed no high charge states without the sextupole field. The ion confinement time in the second stage is 10-15 ms. The measured plasma density of 3×10^{11} cm $^{-3}$, gives $n\tau = 4 \times 10^{9} cm^{-3}$ sec. The beam is extracted from the source by a negative electrode at 10-20 kV. (In practice, the source is biased positive by this amount.) The high charge state beam currents extracted

are shown in Table 1. The charge state distribution is broader than that of a PIG. The emittances are a reasonable match to accelerator injection systems. A key design feature in the system is the two stages with pumping in between. The first stage generates the plasma while the second high vacuum stage produces the high charge states. The duty factor can be 100%, and life-time is 1000's of hours, since there are no sputtered cathodes to replace.

The disadvantage of this device was its large power consumption of 3 MW, and it has been shut down for that reason. But it pointed the way to the design of ECR sources with higher charge states than the PIG. The clear direction to follow is the duplication of this source with superconducting coils to reduce the power consumption. This path is being followed by some laboratories, but the next version of the two stage ECR source to operate was the compact version called MicroMAFIOS.

The MicroMAFIOS is shown in Fig. 29. It was built as a cooperative project of CEN Grenoble, and the cyclotron labs at Louvain, Belgium and Karlsruhe, West Germany. It is now operating in Grenoble. It uses several simplifications to save cost. It is compact in size, uses small bore room temperature solenoid magnets, samarium cobalt permanent magnets for the hexapole, and 10 GHz for both microwave frequencies. The total power is about 100 kW, with 2 kw of UHF

power. Duty factor is 100%. Extraction voltage is up to 8 kV and will be increased to 20 kV in the future. It was expected that the charge states might be lower than for SuperMAFIOS-B due to the smaller size, but fortunately the performance approaches that of the larger source.

The output of the MicroMAFIOS has been analyzed with the magnet of Fig. 30. A sample spectrum of ^{18}O obtained with this magnet is shown in Fig. 31. The use of ^{18}O permits the separation of $^{18}O^{8+}$ from H_2^+. Its intensity is the same as $^{16}O^{8+}$ would be, but the $^{16}O^{8+}$ would be obscured by the H_2^+. The excellent resolution of the analyzing magnet shows all the charge states of ^{18}O, separated from the impurities. The analyzed beam of this source is being used for atomic physics studies of charge exchange cross-sections. Geller has also tried a simpler version called MiniMAFIOS which uses one cavity and one UHF generator. Its start-up is a little more difficult, but its best performance approaches that of MicroMAFIOS.

Several cyclotron laboratories are planning to obtain copies of MicroMAFIOS for external axial injection of high charge state beams. The cyclotron laboratory at Louvain is building a larger ECR source with superconducting solenoid and hexapole coils, called ECREVIS (Jo 79). Tests of a 1/3 scale superconducting model are also planned. The Julich cyclotron plans a similar source. The cyclotron laboratory at Karlsruhe is building a source called HISKA (Be 79) which uses

superconducting and room temperature solenoid coils, together with a samarium cobalt permanent magnet hexapole. This gives a simpler superconducting coil system than at Louvain, but not as high a field in the hexapole. While awaiting the full scale source, a small 2-stage source similar to MicroMAFIOS is being developed. Work is also underway at GSI, Darmstadt to develop an ECR source for high current and medium charge state: 100 μA of U^{10+} for injection into the UNILAC. An advantage of the ECR over the PIG now in use is a longer lifetime.

The direction for future improvements in ECR sources is toward higher extraction voltage from MicroMAFIOS, higher microwave frequency in the larger sources allowing higher plasma density, and further studies of the confinement mechanism and plasma potential well in this promising advanced source.

4.3.2. The Electron Beam Ion Source (EBIS)

The concept of the EBIS to produce high charge states was pioneered by Donets in Dubna starting in 1967, with the first experimental results on EBIS reported in 1969 (Do 69). A history of the EBIS development is given by Donets (Do 76b), including EBIS-2 in 1970 and the two cryogenic versions KRION-1 and KRION-2, which have superconducting magnets and 4°K cryopumping. An extensive list of EBIS references is found in a thesis by Hamm (Ha 77).

The principle of the EBIS is illustrated in Fig. 32. Here we see in Fig. 32a an electron gun which launches a small diameter (1 mm) electron beam down the axis of a magnetic solenoid about 1 m long. The beam expands radially as it leaves the solenoid, and stops on the electron collector. The potential along the axis is defined by a number of hollow cylindrical drift tubes. To produce ions, gas is injected into one of the drift tubes, and stepwise ionization begins. The ions are contained radially in the electrostatic potential well of the electron beam, and axially by positive potential barriers on the end drift tubes as shown in the potential distribution of Fig. 32b. During a short "injection" period, the desired number of ions is accumulated in the well by ionization of the continuous gas feed. Then the potential distribution is switched to the "ionization" mode, in which the first barrier is moved downstream to prevent additional low charge state ions from entering the potential well. The ions reach progressively higher charge states as the contain-

ment continues. After a sufficient time, when the average charge state has reached the desired value, the potential distribution is switched to the "extraction" mode. This applies a ramp voltage on the drift tubes, accelerating the ions out of the source into the extractor and time-of-flight modulation and transport system. The system thus uses a batch type pulsed process in which the intensity is determined by the number of ions per pulse and the number of pulses per second. The maximum number of ions per pulse, N^+, is the number to just neutralize the electron space charge: $\bar{Q}N^+ \leq N^- = IL/v$ where I(A) is electron current, v(cm/s) is electron velocity, and L(cm) is source length. This can be written as:

$$QN^+ \leq N^- = 10^{11} IV^{-\frac{1}{2}} L \qquad (4)$$

where V is the electron beam energy in volts. For example, if I = 1A, V = 10^4 volts and L = 100 cm, $N^+ = 10^{11}/Q$. The KRION-1 is used as an injector for ions such as C^{6+} and N^{7+} into the Dubna synchrotron.

The ion spectra obtained with the time-of-flight analyzer of KRION-2 is shown in Fig. 33. This source has $4^{\circ}K$ cryopumping on the drift tubes, giving 10^{-12} torr in the electron beam region. Here we see in each frame extracted ion pulses displayed on a time scale where the ions are sorted by their charge/mass ratio, with the high charge/mass ions arriving first. For each element a series of extraction frames are shown each with a longer ionization time. These ionization times are, for example, .4-89 ms for carbon, and 1.6-1999 ms for argon. Spectra

like these, with ionization times up to 2 s, indicate excellent operation of the gas pulsing and cryopumping systems, since very low background is seen. In other measurements Kr^{34+} and Xe^{48+} were obtained, with $j\tau = 3 \times 10^{21} cm^{-2}$ and an electron energy of 18 keV. With this type of source, the value of $j\tau$ is known, so that the stepwise electron bombardment ionization cross-sections can be deduced. They have been found to agree reasonably well with the estimates of Lotz (Sec. 2.1.).

The construction of a successful EBIS requires a precisely straight magnetic axis, good alignment of the electron gun with the axis, a high vacuum (10^{-10} torr) and a gas pulsing system. A number of EBIS projects have had difficulty with reliable production of high charge state beams, because one or more of the above requirements were not met. The production of beams from solid material feed systems appears feasible with pulsed laser vaporization or by ion injection through the cathode.

Another EBIS design is the CRYEBIS built by Orsay (Ar 76) as an injector for the Saturne-II synchrotron at Saclay. This source is the culmination of a development program at Orsay during the 1970's. It is shown schematically in Fig. 34. The special features of this source include an external electron gun, and modes of operation for heavy ions and polarized ions. The external gun is used to compress the electron beam electrostatically and then magnetically as it enters the solenoid magnet, to create a high electron beam density, j, in the ionization region. The electron gun is shown in Fig. 35, along with

the electron trajectories, electrostatic equipotential lines, and magnetic field along the axis. A high value of the magnetic field (Fig. 34) is used to obtain high compression for heavy ions using the Dubna gas injection system. A lower value of field is used for the case of polarized neutral atomic beam coming through a hole in the cathode. Here the electron beam must be larger to match the size of the atomic beam. A photograph of the CRYEBIS is shown in Fig. 36.

A surprising result from CRYEBIS was reported by the Orsay group in 1979 (Ar 79). The production of high charge states such as Kr^{34+} and Xe^{44+} occurred in the very short confinement time of 5 ms, Table 2. This time was much shorter than expected, even with the compressed electron beam. From the calculated $j\tau$ values (Fig. 4), j values of up to 10^5A cm^{-2} are deduced. This supercompression of the electron beam might be explained by space charge compensation by the positive ions created, since calculations of electron beam trajectories were made without neutralization. Such a short confinement time would allow fast pulsing of the source at 100 Hz, which would then provide good intensities for injection into cyclotrons or an accumulator ring for a synchrotron. Unfortunately, there has been difficulty repeating these unusual results after CRYEBIS was moved. The alignment requirements would be extremely stringent for this super-compressed electron beam of .01 mm diameter.

Another version of the EBIS source is the time-of-flight EBIS or TOFEBIS built by the Frankfurt group, shown in Fig. 37. In this source, ions form at one end from a neutral feed system, and are ionized in a step-by-step fashion as they drift down a potential ramp to the extraction end. They are then extracted without any containment. A large potential ramp slope produces a fast ion transit giving short ionization time and thus lower charge states, but high current. A flatter ramp gives higher charge states but lower current. The charge state distribution of a TOFEBIS is similar to that of a PIG source. A TOFEBIS is used at the University of Giessen to form high charge state beams for charge exchange experiments (Cl 75b).

A number of other groups have developed EBIS sources. The University of Frankfurt has followed their TOFEBIS work with the design and construction of a 1 m long cryogenic EBIS with a 5T superconducting magnet with cold bore for cryopumping (Be 77). Texas A&M University built a 20 cm long room temperature EBIS with an external high compression gun and with liquid nitrogen trap pumping for injection into their 88-Inch cyclotron. The background pressure was high, giving short electron beam neutralization time of 1 ms and a charge state distribution similar to a PIG source. The CERN group made theoretical and experimental studies of a high compression electron beam going into a 1 m long solenoid (Fo 77). The aim was the production of Ar^{18+} for CERN synchrotron injection, but the program has terminated. The Cornell group is testing a 50 cm long EBIS

with an external high compression electron gun and distributed sputter ion pumping, to be used for atomic physics charge exchange cross-section measurements (Ko 81). A group at Lawrence Berkeley Laboratory is developing a bench test model with a high compression gun and a 10 kG solenoid to understand the super-high compression mode observed by Orsay, and evaluate the geometric and magnetic field alignment requirements (Br 80). The application would be injection into the 88-Inch Cyclotron, which requires a high compression, high repetition rate mode of operation. There is also a Japanese program to construct a cryogenic EBIS called CRYONICE. A recent summary of the physics of EBIS has been written by Vella (Ve 81).

4.4. Short Pulse Sources

There are several interesting sources which produce very short ion pulses from high pulsed power in solids or gases. High charge states are produced by many of these sources such as spark sources, exploding wire sources, laser beams on solids, and plasma focus discharges. The vacuum spark developed, for example, at NRL for atomic spectroscopy studies, discharges a 14 kV capacitor across a 6 mm gap in 2 μs, with 100 kA current (Li 71). Charge states up to Ti^{21+} and Fe^{25+} were observed. NRL has also developed the exploding wire technique for spectroscopic research (Mo 75). In this source, a thin wire, 10^{-3}-10^{-2} cm diameter, is stretched across an electrode gap in vacuum. A 1 MV generator discharges 50 kJ of high energy

electrons in 80 ns, giving a current of 1 MA, through the plasma formed by the vaporizing wire. Charge states up to Cu^{27+} and Au^{51+} were seen (Bu 77).

High density laser pulses on solids also create high charge state ions. This field was reviewed by Tonon (To 72). The energy distribution of cobalt ions for each charge state, from the work of Bykovski et al., is shown in Fig. 38 (To 72). The energy is approximately proportional to charge state. In Fig. 39 is shown the variation of ε = charge/mass with atomic number and laser power density, with measured points and calculated lines. The lines show the benefit of high laser power density in obtaining high ε. In Fig. 40 we see a layout of an extraction system in which the laser target is biased to +100 kV and the extractor is at ground potential. Since the highest charge states are concentrated in a plume perpendicular to the target, the extractor aperture would be centered in that direction if the highest ε were required. There have been other groups developing laser production of high charge states. The review by Peacock (Pe 76) mentions that charge states such as Mg^{11+}, Ti^{20+}, Fe^{23+} and W^{55+} were produced by 1 ns laser pulses at power densities of 5×10^{14} W cm^{-2}. Spectroscopy research is being done by the Naval Research Laboratory with a 30 J, .9 ns laser with a power density of $3 \times 10^{14} Wcm^{-2}$ (Bu 80), to verify the transitions seen in Tokamaks in $Mo^{12+...17+}$. A group at the University of Arkansas uses a 0.3J laser with 10^{11} W cm^{-2} target power, 50 Hz

repetition rate, to generate a plasma plume. It is formed into a beam by a 15 kV extraction gap, and then focused and analyzed (Hu 80). The laser pulse length is 15 ns but the ion beam plume lasts much longer, about 10 μs. Carbon, aluminum, copper and lead targets have been used, with charge states up to C^{5+} and Al^{7+} observed.

Another type of experiment is a gas triggered "z-pinch" vacuum discharge (Bu 79). Here a fast valve lets a puff of gas into a 30 kV 9 mm gap, and triggers a discharge of 300 kA. The plasma is pinched to 0.1 mm diameter. Charge states such as Kr^{27+} were seen spectroscopically. Another similar experiment is with a plasma focus discharge (Rh 81). The initial analysis showed the surprising result that the helium, nitrogen and argon beams were fully stripped. Recently a recalibration of the spectrometer and a track shape analysis showed that the ions were protons (Rh 82). Work is continuing on analysis of other charge/mass species which have been observed.

The research in collective ion acceleration has demonstrated the ability of high current pulsed relativistic electron beams to produce and accelerate ions. This field was reviewed by Reiser (Re 79). Here a 1 MV pulse causes field emission of electrons from a cathode with currents of

10-100 kA, with length 20-100 ns. The ions come either from the anode, a puff of gas, or a laser plume. The University of Maryland group reports ions from hydrogen to xenon to be produced by the electron beam and accelerated by the potential well of the electron up to 5 MeV/nucleon (Fl 81). Graybill reported formation and acceleration of 10^{10}-10^{11} ions/pulse of $N^{4+...6+}$ and $Ar^{6+...12+}$ to energies of 10-20 MeV (Gr 72). Further development of this technique, including high repetition rate capability, could provide an inexpensive ion injector for present accelerators.

The program of development for light ion fusion power reactors requires 10^{14} W to be delivered to a target less than 1 cm in diameter for about 10 ns (Hu 80b). Ions in the mass range 1-20 are under consideration. The heavier ones have the advantage of less current required because of the greater energy per particle for a given range in the pellet, and they are deflected less by the electromagnetic fields of other converging beams. High intensity pulsed sources must be developed for these systems, such as the Sandia plasma gun which produces 10^{17}-10^{18} multiply charged carbon ions traveling about 10^{7} cm s^{-1} (Me 80).

5. CONCLUSION

We have reviewed the principles of ion production, and the types of sources used on many present positive heavy ion accelerators and other systems. Also, we have seen much

new development underway in advanced sources such as the ECR, EBIS, heavy ion fusion, field ionization, and short pulse types. These new developments will certainly open new domains of energies in existing accelerators through higher charge state production, which will serve the needs of many research fields, including nuclear science, atomic physics, fusion power and electronic circuit fabrication.

6. ACKNOWLEDGEMENTS

The author would like to acknowledge with appreciation the generous response to his request for help in preparing this chapter. Among those who contributed references and information were N. Angert, J. Arianer, L. Bex, E. Donets, J. Gavin, R. Geller, L. Glasgow, J.L. Hirshfield, S. Humphries, Y. Jongen, C. Kim, V.O. Kostroun, R.S. Lord, M.L. Mallory, P.A. Miller, Naval Research Laboratory, M. Reiser, M.J. Rhee, H. Schweickert, and J. Watson.

References

Am 76 S. Amiel and G. Engler, eds., Proceedings of the IXth International Conference on Electromagnetic Isotope Separators and Related Ion Accelerators, Nucl. Instrum. Methods 139:1 (1976).

Ar 75 J. Arianer, Proceedings of the 7th International Conference on Cyclotrons and their Applications, Zurich, Birkhauser (1975), p. 341.

Ar 76 J. Arianer and C. Goldstein, IEEE Trans. Nucl. Sci. NS-23, 2:979 (1976).

Ar 77 J. Arianer. A. Cabrespine, G. Deschamps, and C. Goldstein, Proceedings of Workshop on EBIS and Related Topics, Darmstadt, West Germany (1977), p. 17.

Ar 79 J. Arianer, A. Cabrespine, and C. Goldstein, IEEE Trans. Nucl. Sci. NS-26, 3:3713 (1979).

Ba 66 A.P. Banford, The Transport of Charged Particle Beams, Spon, London (1966).

Be 71 J.R.J. Bennett, IEEE Trans. Nucl. Sci. NS-18, 3:55 (1971).

Be 72 H.D. Betz, Rev. Mod. Phys., 44:465 (1972)

Be 72b J.R.J. Bennett, IEEE Trans. Nucl. Sci. NS-19, 2:48 (1972).

Be 76 L. Bex, D.J. Clark, C.E. Ellsworth, R.M. Estrella, R.A. Gough, and W.R. Holley, IEEE Trans. Nucl. Sci. NS-23, 2:1077 (1976).

Be 77 R. Becker, H. Klein, and M. Kleinod, Proceedings of the Workshop on EBIS and Related Topics, Darmstadt, GSI-P-3-77 (1977), p. 35.

Be 79 V. Bechtold, H.P. Ehret, L. Friedrich, J. Mollenbeck, and H. Schweickert, IEEE Trans. Nucl. Sci. NS-26, 3:3680 (1979).

Be 80 L. Bex and G. Cardin, GANIL 80R/153/IS/09, GANIL Laboratory (1980).

Br 79 Alec N. Broers, Physics Today, 32, 11:39 (1979).

Br 80 I.G. Brown, B. Feinberg, and W.B. Kunkel, Bull. Am. Phys. Soc. 25, 8 (1980), P. 957, Abstract 6S1.

Bu 77 P.G. Burkhalter, C.M. Dozier, and D.J. Nagel, Phys. Rev. A 15, 2:700 (1977).

Bu 79 P.G. Burkhalter, J. Shiloh, A. Fisher, and Robert D. Cowan, J. Appl. Phys. 50, 7:4532 (1979).

Bu 80 P.G. Burkhalter, Joseph Reader, and Robert D. Cowan, J. Opt. Soc. Am. 70, 8:912 (1980).

Ca 70 Thomas A. Carlson, C.W. Nestor, Jr., Neil Wassermann, and J.D. McDowell, Atomic Data 2:63 (1970).

Ch 79 Warren Chupp, Dave Clark, Robert Richter, John Staples, and Emery Zajec, IEEE Trans. Nucl. Sci. NS-26, 3:3036 (1979).

Ch 79b Steven Abbott, Warren Chupp, Andris Faltens, William Herrmannsfeldt, Egon Hoyer, Denis Keefe, Charles Hongchul Kim, Stephen Rosenblum, and Joseph Shiloh, IEEE Trans. Nucl. Sci. NS-26, 3:3095 (1979).

Cl 72 D.J. Clark, Rep. Prog. Phys. 35:1007 (1972).

Cl 75 R. Clampitt, K.L. Aitken, and D.K. Jefferies, J. Vac. Sci. Technol. 12:1208 (1975).

Cl 75b G. Clausnitzer, H. Klinger, A. Muller, and E. Salzborn, Nucl. Instrum. Methods 128:1 (1975).

Cl 77 David J. Clark, IEEE Trans. Nucl. Sci. NS-24, 3:1064 (1977).

Da 68 J.D. Daugherty, L. Grodzins, G.S. Janes, and R.H. Levy, Phys. Rev. Letters 20:369 (1968).

De 73 G. Dearnaley, J.H. Freeman, R.S. Nelson, and J. Stephen, Ion Implantation, North Holland (1973), Chap. 4.

Do 69 E.D. Donets, V.I. Ilyuchenko, and V.A. Alpert, Proceedings of the First International Conference on Ion Sources, Saclay (1969), p. 635.

Do 76 G. Doucas, T.J.L. Greenway, H.R. McK. Hyder, and A.B. Knox, IEEE Trans. Nucl. Sci. NS-23, 2:1155 (1976).

Do 76b E.D. Donets, IEEE Trans. Nucl. Sci. NS-23, 2:897 (1976).

Do 80 E.D. Donets and V.P. Ovsyannikov, Report P7-80-515, Joint Institute for Nuclear Research, Dubna, U.S.S.R. (1980).

Do 81 S. Dousson, R. Geller, and B. Jacquot, Low-energy Ion Beams, 1980, Conference Series No. 54, The Institute of Physics, Bristol and London (1981), p. 304.

En 71 J.E. Eninger, Nucl. Instrum. Methods 97:19 (1971)

Fl 81 L.E. Floyd, W.W. Destler, M. Reiser, and H.M. Shin, J. Appl. Phys., 52, 2:693 (1981).

Fo 77 B. Fogen and T.R. Sherwood, Proceedings of the Workshop on EBIS and Related Topics, Darmstadt, GSI-P-3-77 (1977), p. 27.

Ga 76 Basil Gavin, IEEE Trans. Nucl. Sci. NS-23, 2:1008 (1976).

Ga 81 B. Gavin, S. Abbott, R. MacGill, R. Sorensen, J. Staples, and R. Thatcher, IEEE Trans. Nucl. Sci. NS-28, 3:2684 (1981).

Ge 79 R. Geller, IEEE Trans. Nucl. Sci. NS-26, 2:2120 (1979).

Go 79 R.A. Gough, D.J. Clark, and L.R. Glasgow, IEEE Trans. Nucl. Sci. NS-26, 2:2164 (1979).

Gr 72 S.E. Graybill, IEEE Trans. Nucl. Sci. NS-19, 2:292 (1972).

Gr 74 T.S. Green, Rep. Prog. Phys. 37:1257 (1974).

Gr 74b T.S. Green, Proceedings of the Second Symposium on Ion Sources and Formation of Ion Beams, LBL 3399, Lawrence Berkeley Laboratory (1974), p.I-2.

Gr 76 T.S. Green, IEEE Trans. Nucl. Sci. NS-23, 2:918 (1976).

Ha 77 R.W. Hamm, PhD Thesis, Los Alamos Scientific Laboratory, Report LA-7077-T (1977).

Hu 76 E.D. Hudson, M.L. Mallory, and R.S. Lord, IEEE Trans. Nucl. Sci. NS-23, 2:1065 (1976).

Hu 80 R.H. Hughes, R.J. Anderson, C.K. Manka, M.R. Carruth, L.G. Gray, and J.P. Rosenfeld, J. Appl. Phys. 51, 8:4088 (1980).

Hu 80b S. Humphries, Jr., Comments Plasma Phys. Cont. Fusion 6, 1:45 (1980).

Jo 79 Y. Jongen, C. Pirart, G. Ryckewaert, and J. Steyaert, IEEE Trans. Nucl. Sci. NS-26 3:3677 (1979).

Ke 76 R. Keller and M. Muller, IEEE Trans. Nucl. Sci. NS-23, 2:1049 (1976).

Ke 79 Roderich Keller, Radiation Effects 44:201 (1979).

Ke 81 Roderich Keller, Nucl. Instrum. Methods 189:97 (1981).

Kl 76 M. Kleinod, R. Becker, H. Klein, and W. Schmidt, IEEE Trans. Nucl. Sci. NS-23, 2:1023 (1976).

Ko 81 V.O. Kostroun, E. Ghanbari, E.N. Beebe, and S.W. Janson, IEEE Trans. Nucl. Sci. NS-28, 3:2660 (1981).

La 73 L. Jackson Laslett, IEEE Trans. Nucl. Sci. NS-20, 3:271 (1973).

La 74 Lawrence Berkeley Laboratory Research Proposal ERAN-250 (1974), p. 89.

Li 71 T.N. Lie and R.C. Elton, Phys. Rev. A 3, 3:865 (1971).

Lo 68 W. Lotz, Z. Phys. 216:241 (1968).

Lo 81 Jean-Marie Loiseaux, Nucl. Phys. A354:415c (1981).

Me 80 C.W. Mendel, Jr., P.M. Zagar, G.S. Mills, S. Humphries, Jr., and S.A. Goldstein, Rev. Sci. Instrum. 51, 12:1641 (1980).

Mo 75 D. Mosher, S.J. Stephanakis, K. Hain, C.M. Dozier, and F.C. Young, Ann. N.Y. Acad. Sci. 251:632 (1975).

Ol 81 M. Olivier, Proceedings of the Workshop on Accelerator Systems for Relativistic Heavy Ions in Medical and Scientific Research, Medical Accelerator Research Institute, Edmonton, Alberta, Canada (1981).

Or 75 J.H. Orloff and L.W. Swanson, J. Vac. Sci. Technol. 12, 6:1209 (1975).

Pa 72 A.S. Pasyuk and Yu. P. Tretyakov, Proceedings Second International Conference on Ion Sources, Vienna (1972) p. 512.

Pe 37 F.M. Penning, Physica 4:71 (1937).

Pe 76 N.J. Peacock, ed. I. Sellin and D. Pegg, Beam Foil Spectroscopy, 2:925, Plenum Press (1976).

Re 79 Martin P. Reiser, IEEE Trans. Nucl. Sci. NS-26, 2:2427 (1979).

Rh 81 M.J. Rhee, IEEE Trans. Nucl. Sci. NS-28, 3:2663 (1981).

Rh 82 M. J. Rhee, Private communication.

Sc 76 H. Schulte, W. Jacoby, and B.H. Wolf, IEEE Trans. Nucl. Sci. NS-23, 2:1042 (1976).

Se 72 A. Septier, IEEE Trans. Nucl. Sci. NS-19, 2:22 (1972).

Se 79 R.L. Seliger, J.W. Ward, V. Wang, and R.L. Kubena, Appl. Phys. Lett. 34(5):310 (1979).

Si 78 G. Sidenius, Nucl. Instrum. Methods 151:349 (1978).

Th 53 P.C. Thonemann, Prog. Nucl. Phys. 3:219 (1953)

To 72 G.F. Tonon, IEEE Trans. Nucl. Sci. NS-19, 2:172 (1972).

Va 77 L. Vályi, Atom and Ion Sources, John Wiley and Sons, London (1977).

Va 77b L. Vályi, Atom and Ion Sources, John Wiley and Sons, London (1977), p. 26.

Va 77c L. Vályi, Atom and Ion Sources, John Wiley and Sons, London (1977), p. 134.

Va 79 R.P. Vahrenkamp and R.L. Seliger, IEEE Trans. Nucl. Sci. NS-26, 3:3101 (1979).

Ve 81 M.C. Vella, Nucl. Instrum. Methods 187:313 (1981).

Vo 70 E.D. Vorobév and A.S. Pasyuk, Report P7-5177, JINR, Dubna (1970).

Wi 74 H. Winter and B.H. Wolf, Proceedings of the Second Symposium on Ion Sources and Formation of Ion Beams, LBL-3399, Lawrence Berkeley Laboratory (1974), p.V-1.

		PIG	ECR(Sup.MAF.-B)	EBIS
Ion	Q	$I(s^{-1})$	$I(s^{-1})$	$I(pulse^{-1})$
N	2+	$1x10^{15}$		
	5+	$1x10^{13}$	$5x10^{13}$	$2x10^{10}$
	7+		$5x10^{12}$	10^{10}
Ar	3+	$2x10^{15}$		
	8+	$4x10^{12}$	$3x10^{13}$	10^{10}
	12+		10^{12}	$8x10^{9}$
	18+			$6x10^{9}$
Xe	3+	$2x10^{14}$		
	10+	$1x10^{12}$	$4x10^{12}$	10^{10}
	26+		$4x10^{10}$	$4x10^{9}$
	44+			$2x10^{9}$
Norm. Emit. ε_n (π mm mrad)		.1-1	.1-1	.1

Table 1. Some typical beam intensities from several high charge state heavy ion sources. PIG data is for 15 hour average from Bex (Be 80). ECR data is from Geller (Ge 79). EBIS intensities are calculated as $I = 10^{M}/Q$ per pulse. EBIS repetition rate could be $1\text{-}10^{3}$ Hz, with the higher rate corresponding to lower charge states and short confinement times.

Electron beam parameters	3.8 keV 0.19A	4.5 keV 0.25A	6.5 keV 0.6A	4.8 keV 0.33A	4.8 keV 0.33A
Ion, Maximum charge state	N^{7+}	Ne^{10+}	Ar^{18+}	Kr^{34+}	Xe^{44+}
Containment time	6 ms	7 ms	8 ms	5 ms	5 ms
Abundance in the spectrum	100%	100%	>70%	70%	10%
Number of particles per pulse	$5x10^9$	$3x10^9$	$2x10^8$	$2x10^8$	$3x10^7$

Table 2. Experimental data obtained with supercompression mode of CRYEBIS source (Ar 79).

Figure Captions

1. Total ionization potentials for charge states shown on plots. Data is from Carlson et al.(Ca 70). Courtesy Oak Ridge National Laboratory.
2. Electron impact ionization cross-sections for some common gases versus electron energy, from Valyi (Va 77b).
3. Charge state fraction for argon plotted versus the ionization factor $J\tau$ for bombardment with 10 keV electrons. (Ol 81).
4. Charge to mass ratio, Q/A, obtained when atom of number Z is bombarded with 10 keV electrons with ionization factor $J\tau$. (Ol 81).
5. Operating regions of ion sources used in present accelerators, and advanced high charge state ion sources.
6. Charge states produced by various ion sources, plasma devices, and strippers (Cl 77).
7. Surface ionization current density versus temperature. First symbol is projectile atom; second is surface material. (Va 77c).
8. Ion source beam emittance measuring system used by the Oxford University Nuclear Physics Laboratory. A measurement takes about 7 minutes (Do 76).
9. Ion source beam emittance plot, with brightness contours, obtained with the system of Fig. 8 (Do 76).

10. Ion source beam emittance plot, showing aberration, obtained with the system of Fig. 8 (Do 76).
11. Beam emittance measuring system used for an external PIG source at the Lawrence Berkeley Laboratory 88-Inch Cyclotron. A measurement takes about 0.5 s (Be 76).
12. Beam emittance storage oscilloscope data and emittance plot obtained with system of Fig. 11 (Be 76).
13. Retarding field energy analyzer for negative ion source beams used at the Oxford University Nuclear Physics Laboratory (Do 76). An integral spectrum is produced.
14. Ion beam differential energy spectrum obtained by differentiating data from the system of Fig. 13 (Do 76).
15. The Penning discharge source developed by Hughes Research Laboratories for heavy ion fusion application. It produces low emittance Xe^{1+} beams of 30 mA intensity with a single extraction aperture (Va 79).
16. Multi-aperture source developed at Lawrence Berkeley Laboratory for 30 mA of Xe^{1+} for heavy ion fusion applications. Accel-decel extraction is used (Ch 79).
17. Multi-aperture source developed at GSI to produce 50 mA of Xe^{1+} for heavy ion fusion work. Magnetic confinement and accel-decel extraction are used (Ke 81).
18. Large area surface ionization Cs^{1+} source of Lawrence Berkeley Laboratory for pulsed 1 A beam. Purpose is heavy ion fusion (Ch 79b).

19. High brightness electric field ionization source developed by Hughes Research Laboratories for microcircuit fabrication. Focused beams of 1000-5000 Å diameter were obtained (Se 79).
20. Schematic diagram of PIG source with arc-heated cathodes and side extraction.
21. Dubna internal cyclotron PIG source with indirectly heated upper cathode and sputter electrode for solid material feed. It is inserted through midplane gap (Pa 72).
22. PIG source used at the UNILAC heavy ion linear accelerator at GSI, Darmstadt, West Germany (Sc 76).
23. Compact PIG source used in the 2.5 MV pressurized dynamitron injector at the Lawrence Berkeley Laboratory SuperHILAC heavy ion linear accelerator (Ga 76).
24. PIG source used internally at the Lawrence Berkeley Laboratory 88-Inch Cyclotron. It is inserted axially through lower pole (Go 79).
25. Internal cyclotron PIG source solid feed system using back bombardment sputtering by decelerated low charge states, developed at the Oak Ridge National Laboratory ORIC Cyclotron (Hu 76).
26. Duoplasmatron source developed at GSI to inject high charge state heavy ions into the UNILAC (Ke 76).
27. Details of electrodes (IE = intermediate electrode, A = anode) of three GSI duoplasmatron sources. The magnetic field on axis is plotted, and the plasma boundary is

sketched (Ke 76).

28. The SuperMAFIOS-B ECR source of Geller at Grenoble. Before it was shut down, this large plasma machine demonstrated high charge state production with its two ionization stages (Ge 79).

29. The ECR source MicroMAFIOS at Grenoble. This compact two-stage source gives almost the same charge states as SuperMAFIOS-B (Do 81).

30. Analyzing magnet system used with the MicroMAFIOS source of Fig. 29 to resolve high charge state beams (Do 81).

31. Ion spectra obtained with MicroMAFIOS source of Fig. 29 using analyzing system of Fig. 30. The detection of fully stripped oxygen was made possible by use of ^{18}O source gas, to separate it from H_2^+ (Do 81).

32. Schematic drawing of KRION ion source of the EBIS type, developed at Dubna. Electron gun is inside solenoid magnet (Do 76b).

33. Recent experimental data obtained with KRION-2 source at Dubna. Charge distributions from time-of-flight analyzer are shown for several ionization times for each element (Do 80).

34. Sketches of the EBIS source named CRYEBIS, built at Orsay. The axial distribution of magnetic field is shown at top, and the distribution of electrode voltage is shown at bottom. Electron gun is external to

solenoid (Ar 77).

35. Electron gun, electron beam and equipotential lines for Orsay CRYEBIS source of Fig. 34 (Ar 76).

36. Photograph of Orsay CRYEBIS source. Beam travels from gun at left through superconducting solenoid at center, to extraction, focusing and 90 degree bend at right. Courtesy of J. Arianer, Orsay.

37. The principle of the Time-of-Flight EBIS or TOFEBIS suggested by the Frankfurt group. Ions drift axially along the electron beam without confinement barriers (Kl 76).

38. Energy distribution of cobalt ions with laser flux of $10^{13} W/cm^2$ according to Bykovski et al., as shown by Tonon (To 72).

39. Variation of $\varepsilon = Q/A$ with ion atomic number A.N. = Z and laser density (To 72).

40. Extraction system for laser ion source designed by Tonon and Rabeau, discussed by Tonon (To 72).

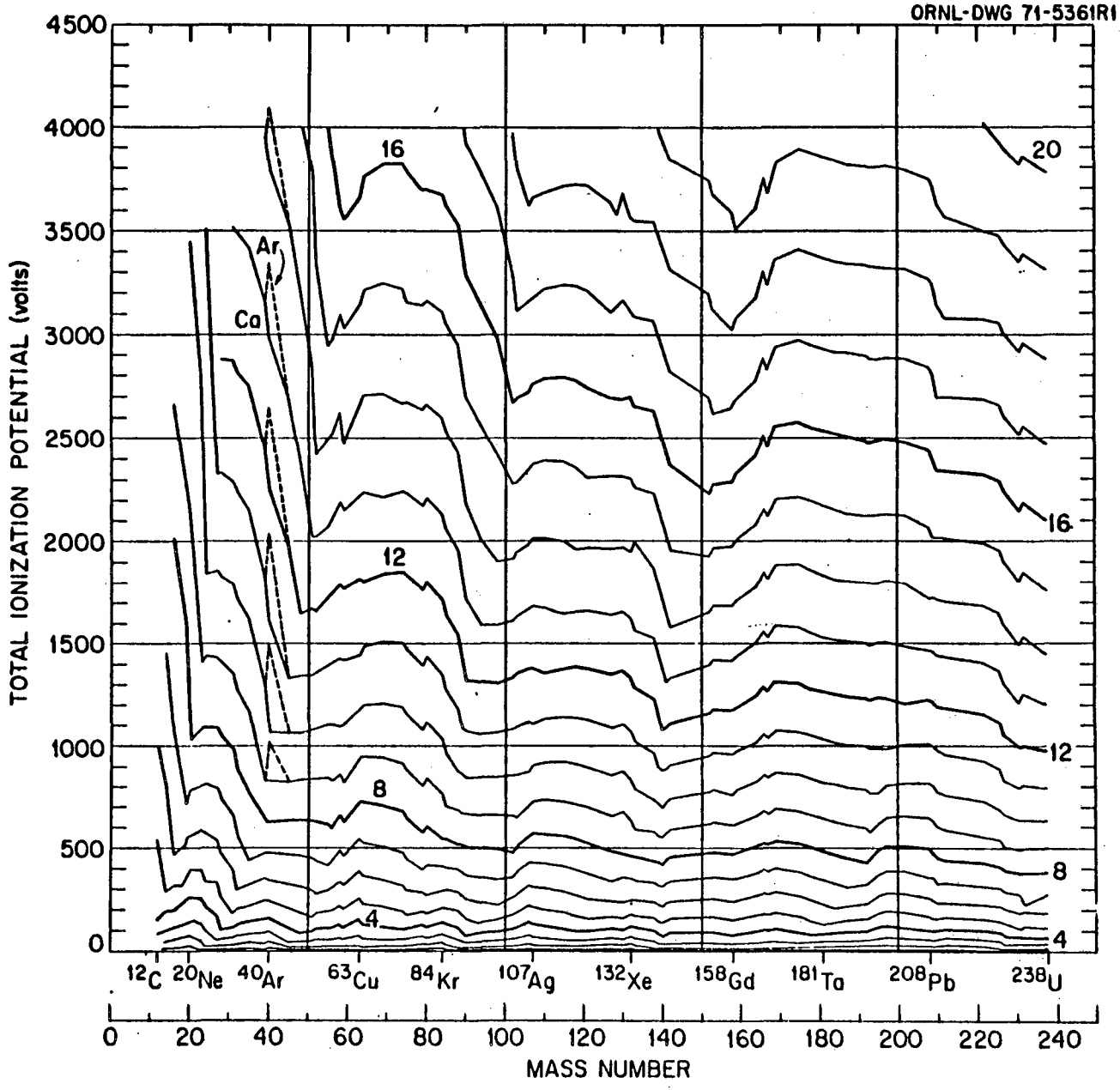
ORNL-DWG 71-5361R1
TOTAL IONIZATION POTENTIAL (volts)
4500
4000
3500
3000
2500
2000
1500
1000
500
0
Ar
Ca
16
12
8
4
20
16
12
8
4
^{12}C ^{20}Ne ^{40}Ar ^{63}Cu ^{84}Kr ^{107}Ag ^{132}Xe ^{158}Gd ^{181}Ta ^{208}Pb ^{238}U
0 20 40 60 80 100 120 140 160 180 200 220 240
MASS NUMBER

Figure 1.

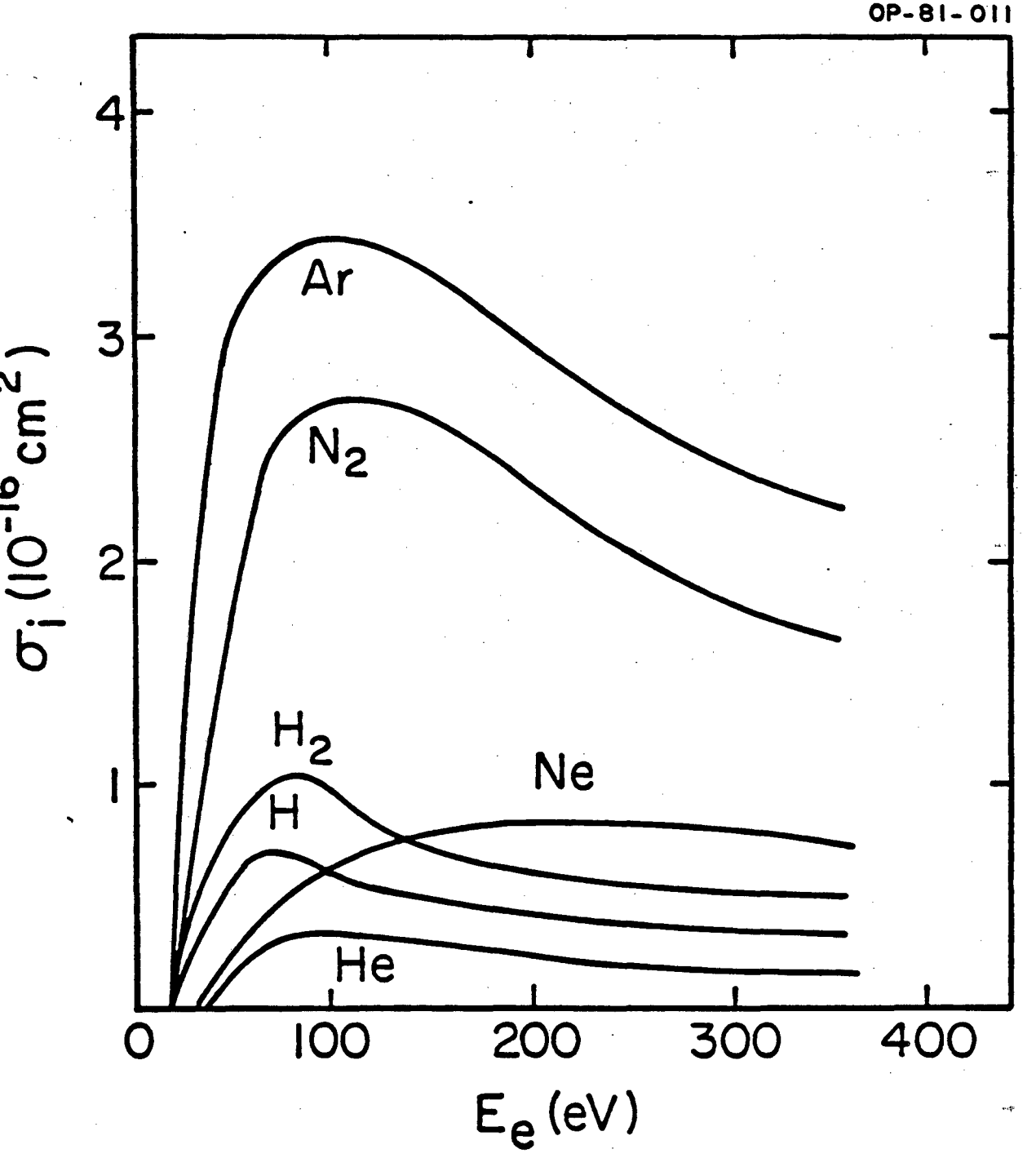

Figure 2.

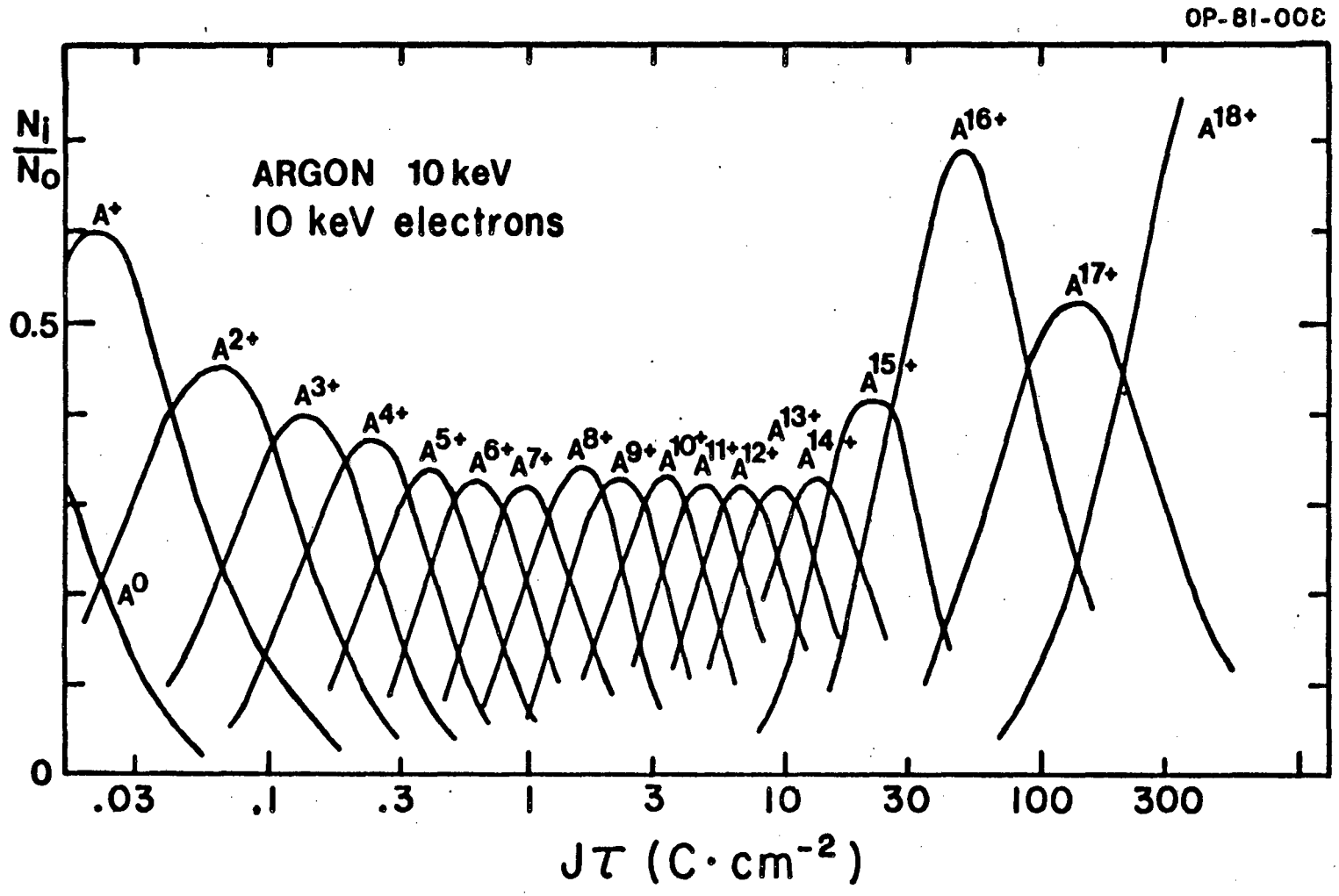
OP-81-006
$\frac{N_i}{N_o}$
ARGON 10 keV
10 keV electrons
A^0
A^+
A^{2+}
A^{3+}
A^{4+}
A^{5+}
A^{6+}
A^{7+}
A^{8+}
A^{9+}
A^{10+}
A^{11+}
A^{12+}
A^{13+}
A^{14+}
A^{15+}
A^{16+}
A^{17+}
A^{18+}
0
0.5
.03
.1
.3
1
3
10
30
100
300
$J\tau$ (C·cm^{-2})

Figure 3.

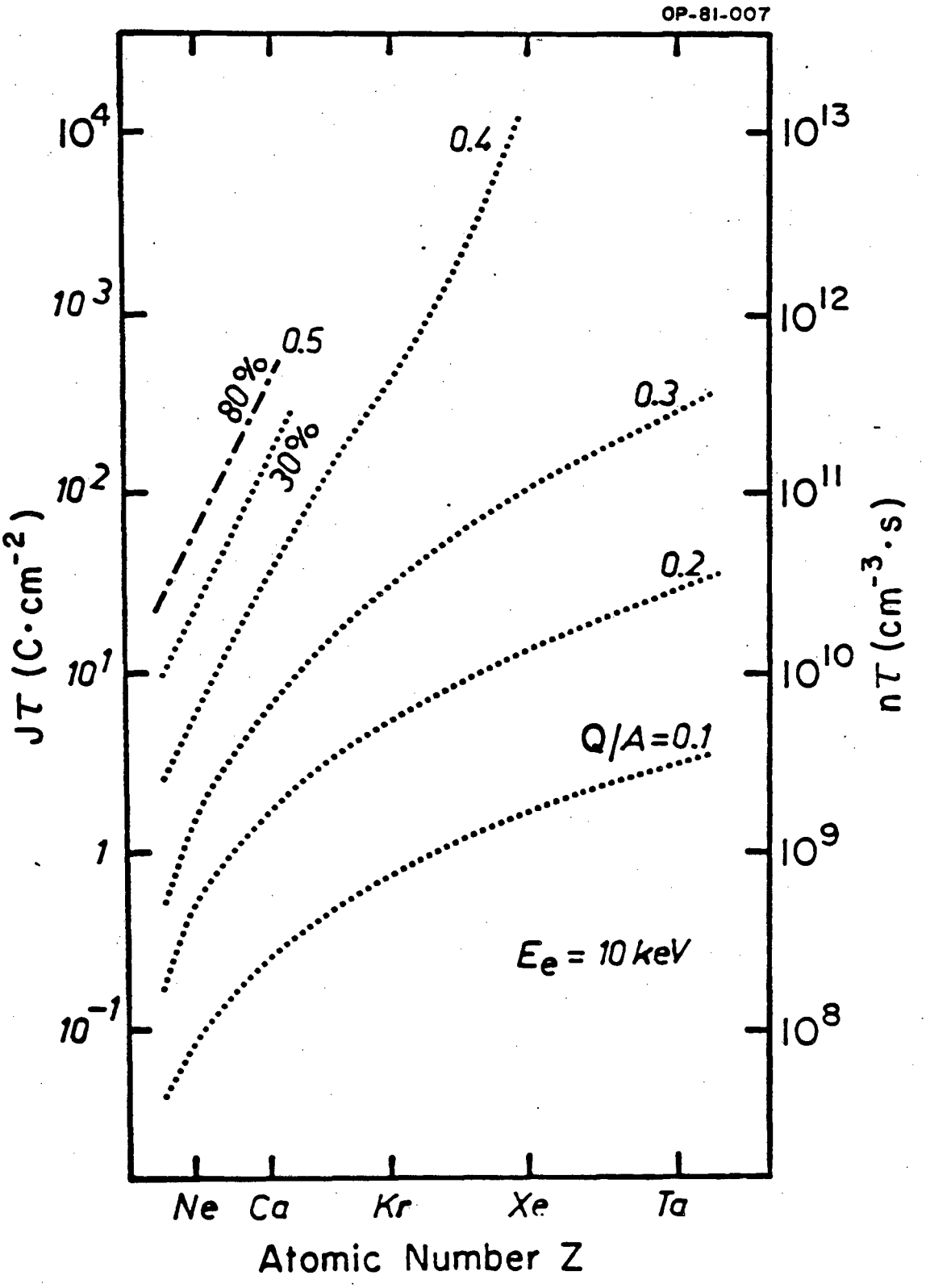
OP-81-007
10^4
10^3
10^2
10^1
1
10^{-1}
$J\tau$ (C·cm^{-2})
10^{13}
10^{12}
10^{11}
10^{10}
10^9
10^8
$n\tau$ (cm^{-3}·s)
0.4
0.5
80%
30%
0.3
0.2
Q/A=0.1
E_e = 10 keV
Ne
Ca
Kr
Xe
Ta
Atomic Number Z

Figure 4.

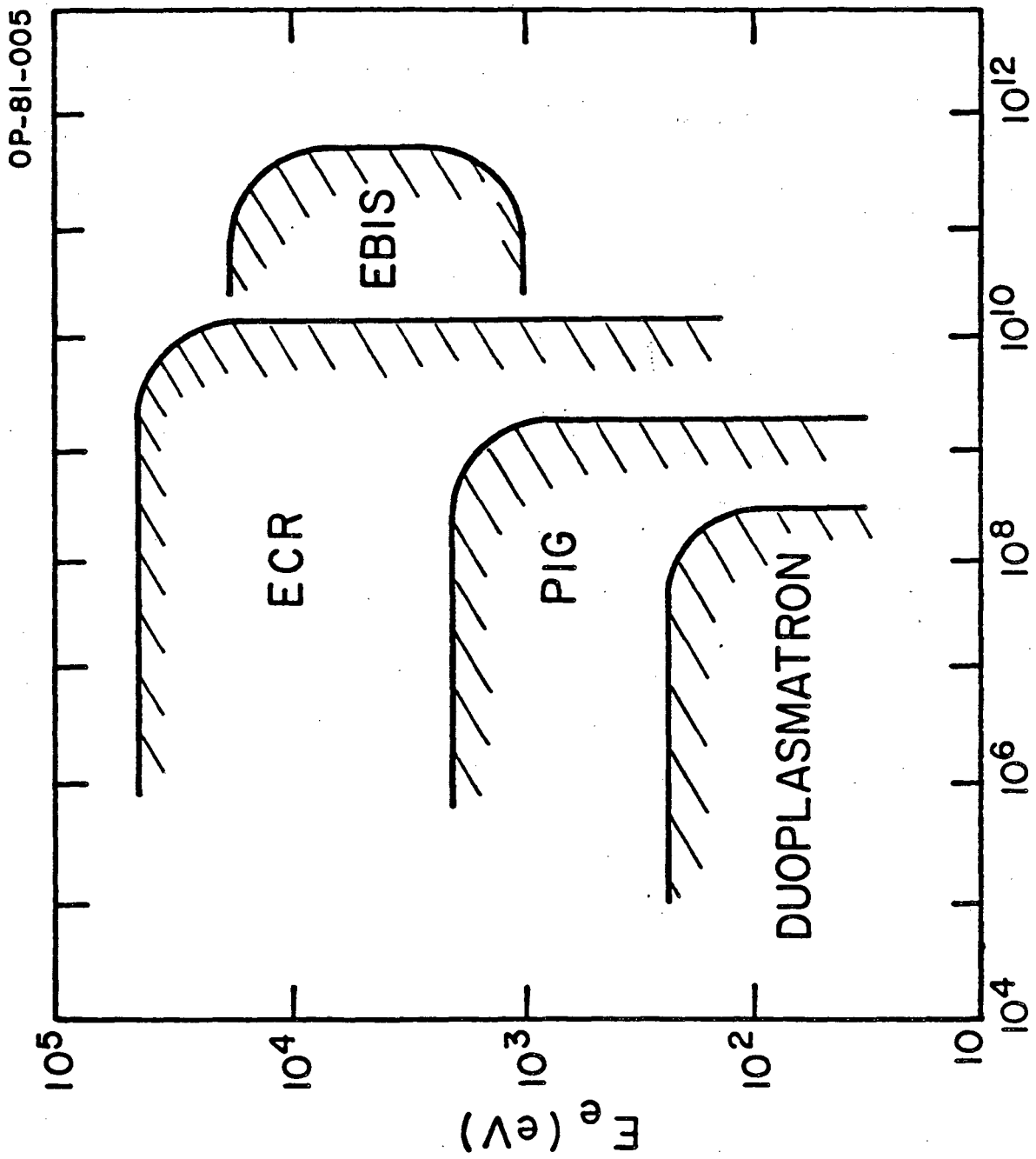
OP-81-005
EBIS
ECR
PIG
DUOPLASMATRON
10^5
10^4
10^3
10^2
10
10^4
10^6
10^8
10^{10}
10^{12}
T_e (eV)
$n\tau$ ($cm^{-3}.s$)

Figure 5.

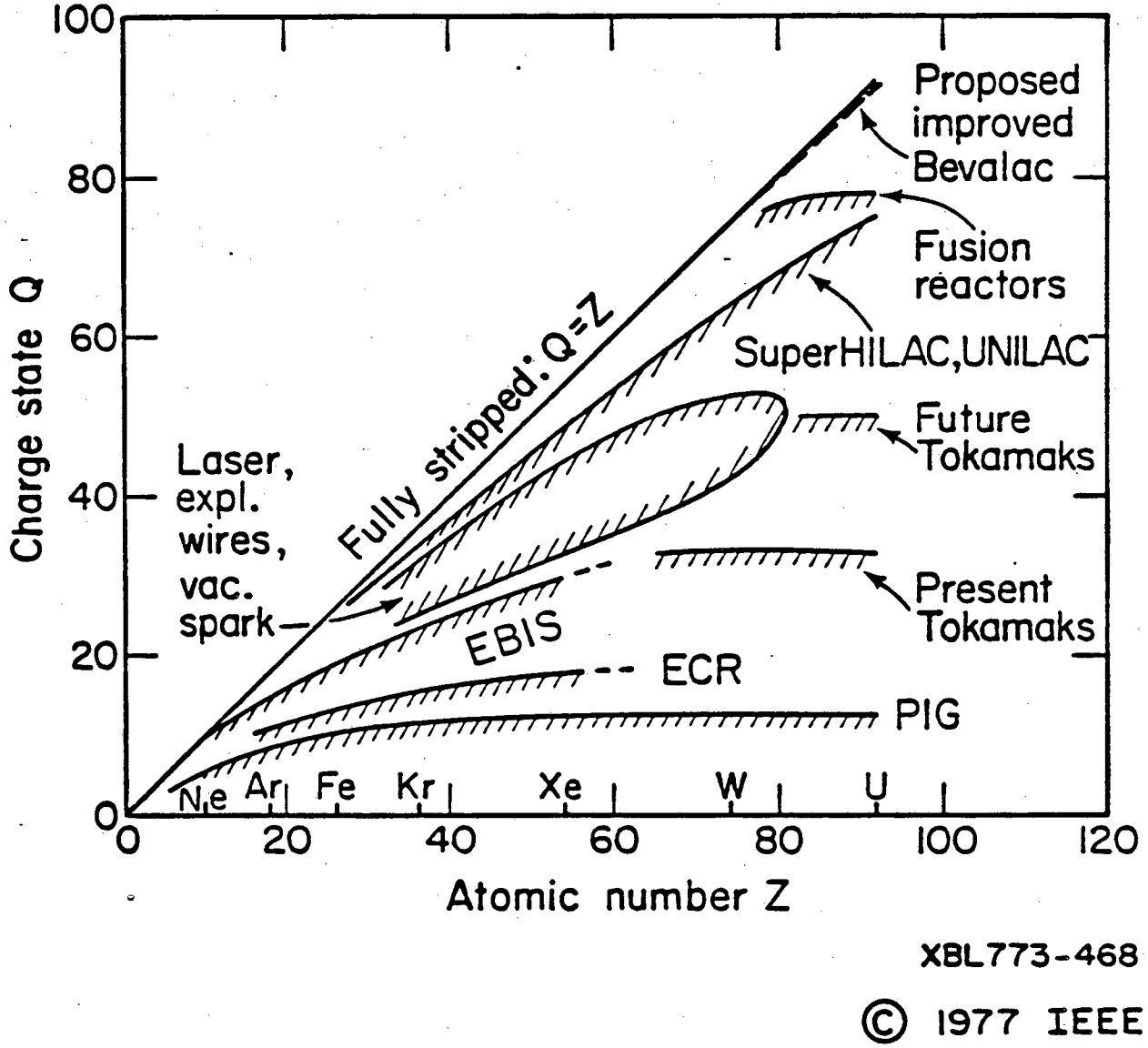

XBL773-468

Figure 6.

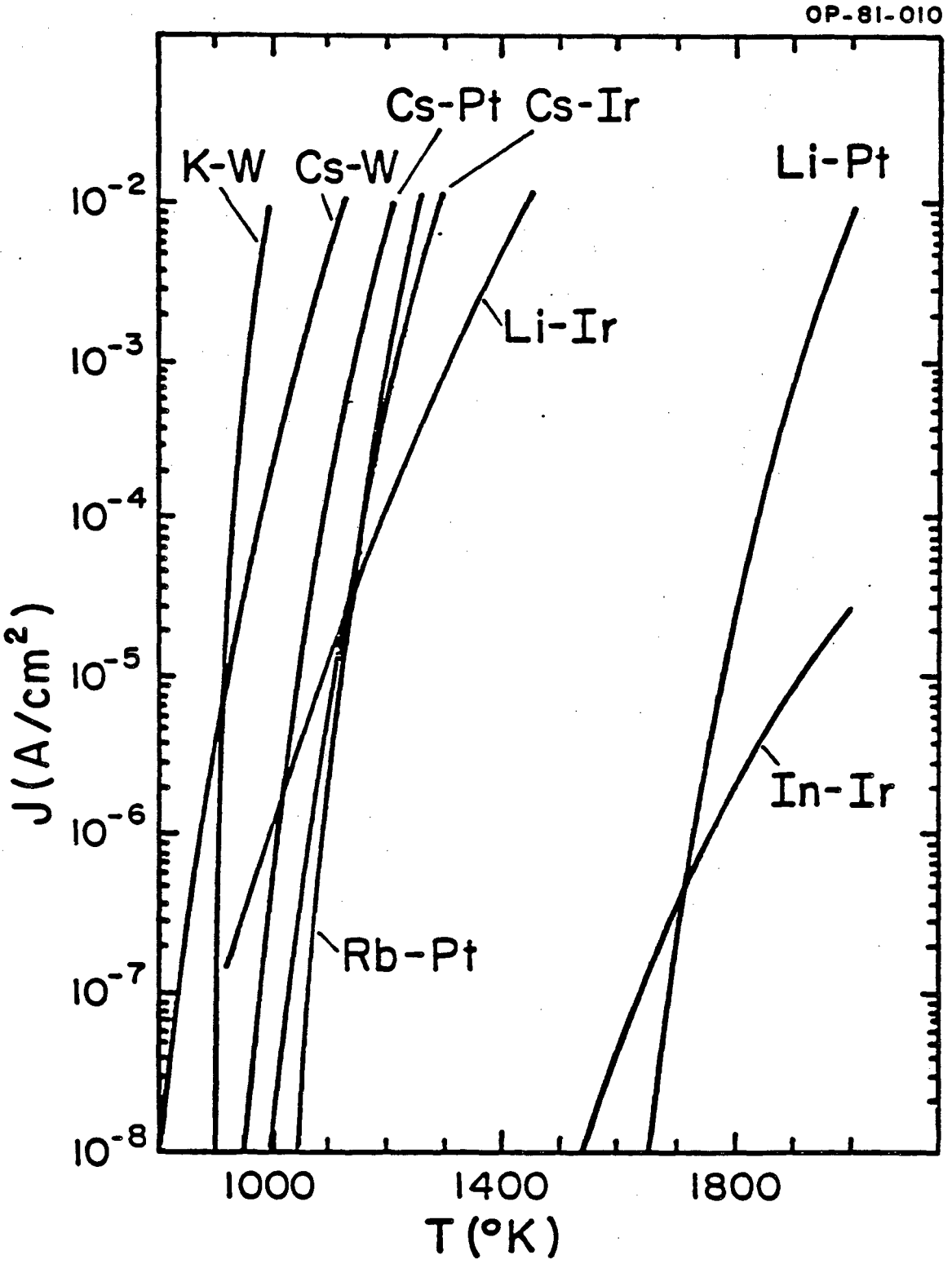
OP-81-010
Cs-Pt
Cs-Ir
K-W
Cs-W
Li-Pt
Li-Ir
In-Ir
Rb-Pt
10^{-2}
10^{-3}
10^{-4}
10^{-5}
10^{-6}
10^{-7}
10^{-8}
J(A/cm²)
1000
1400
1800
T(°K)

Figure 7.

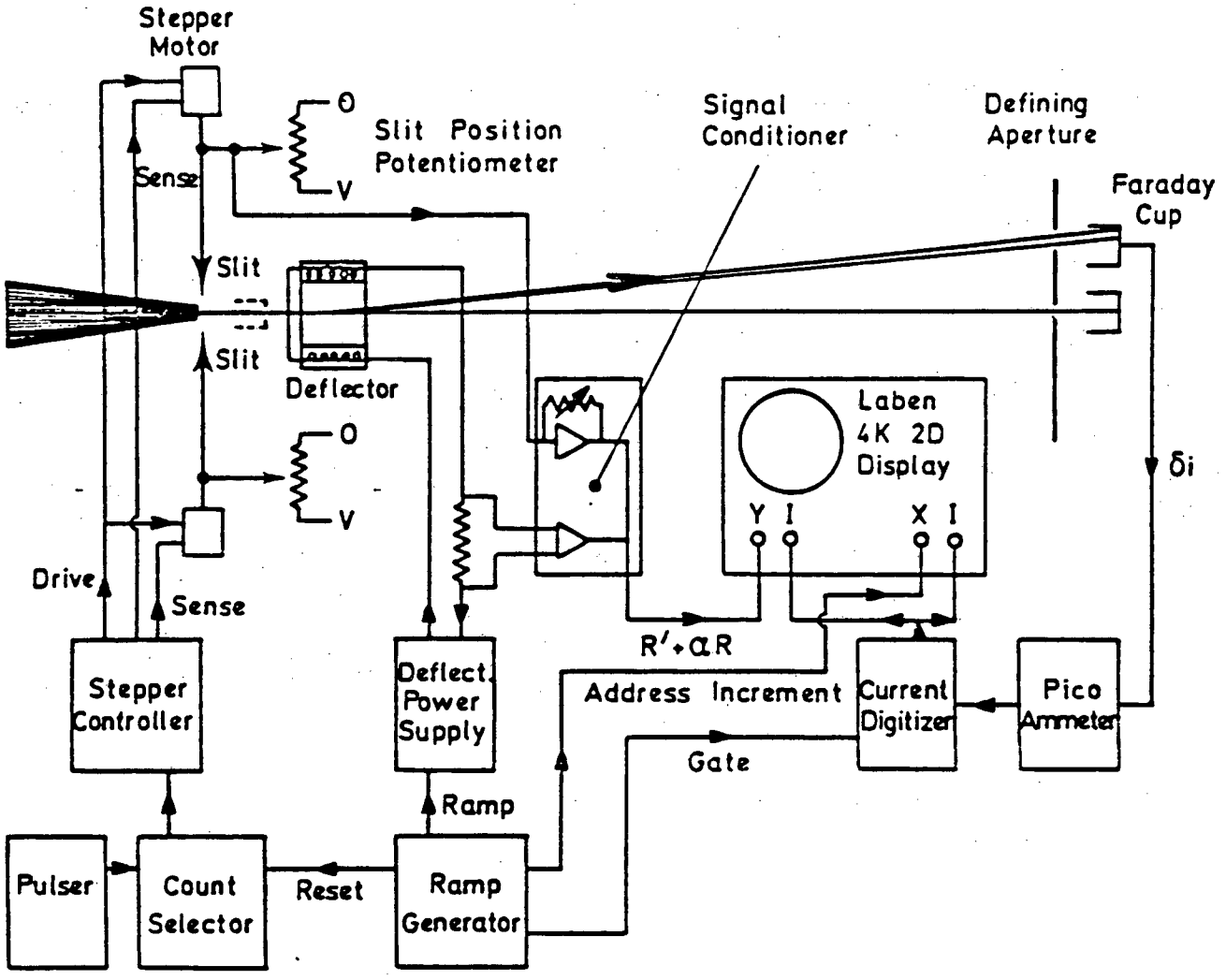

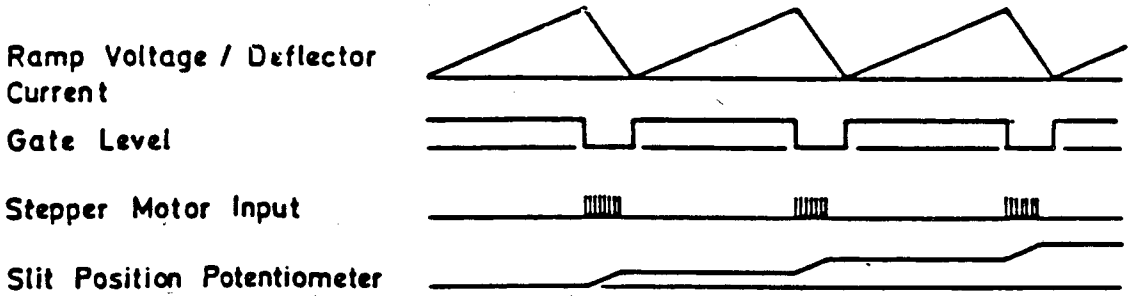

Figure 8.

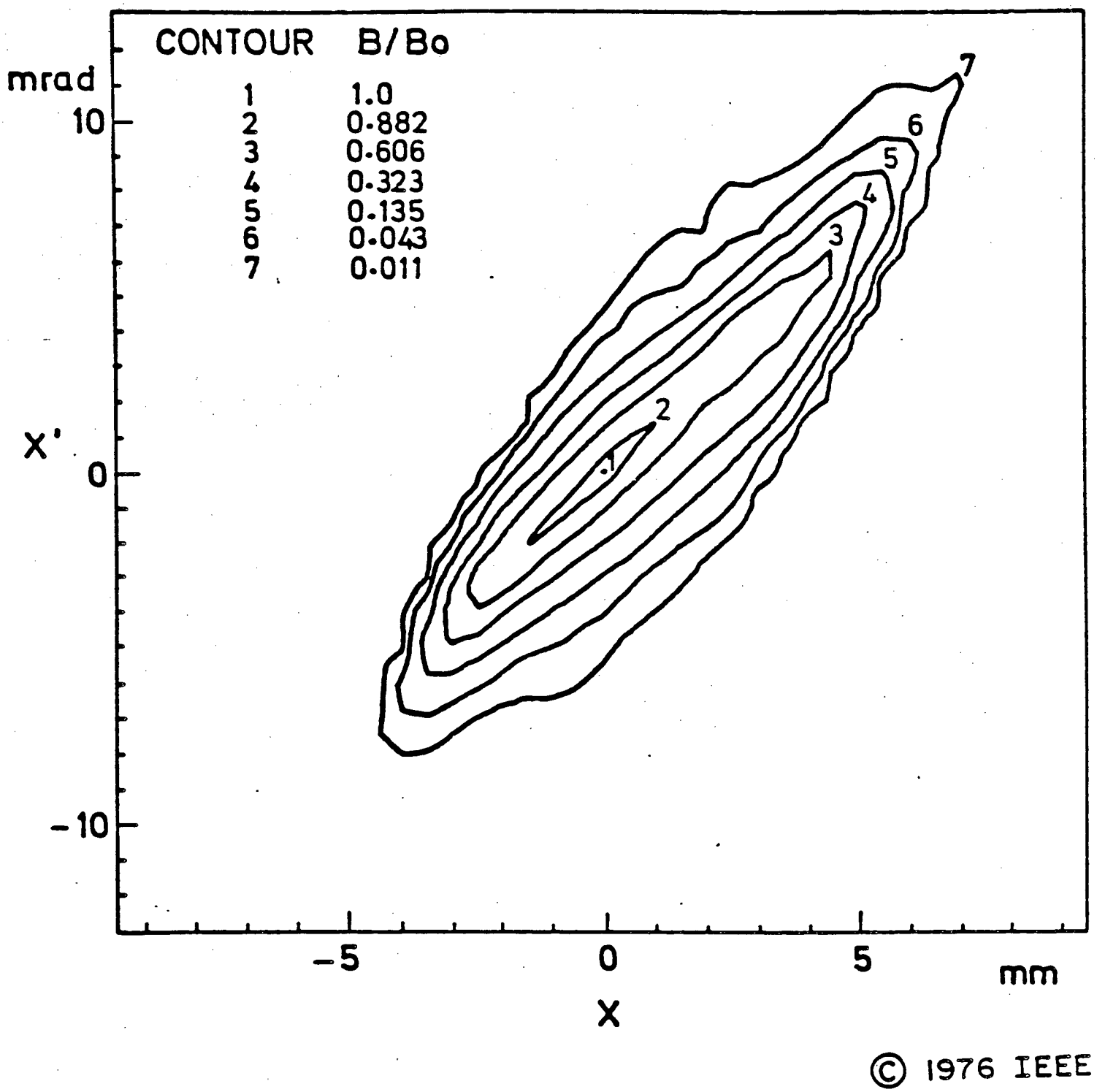

Figure 9.

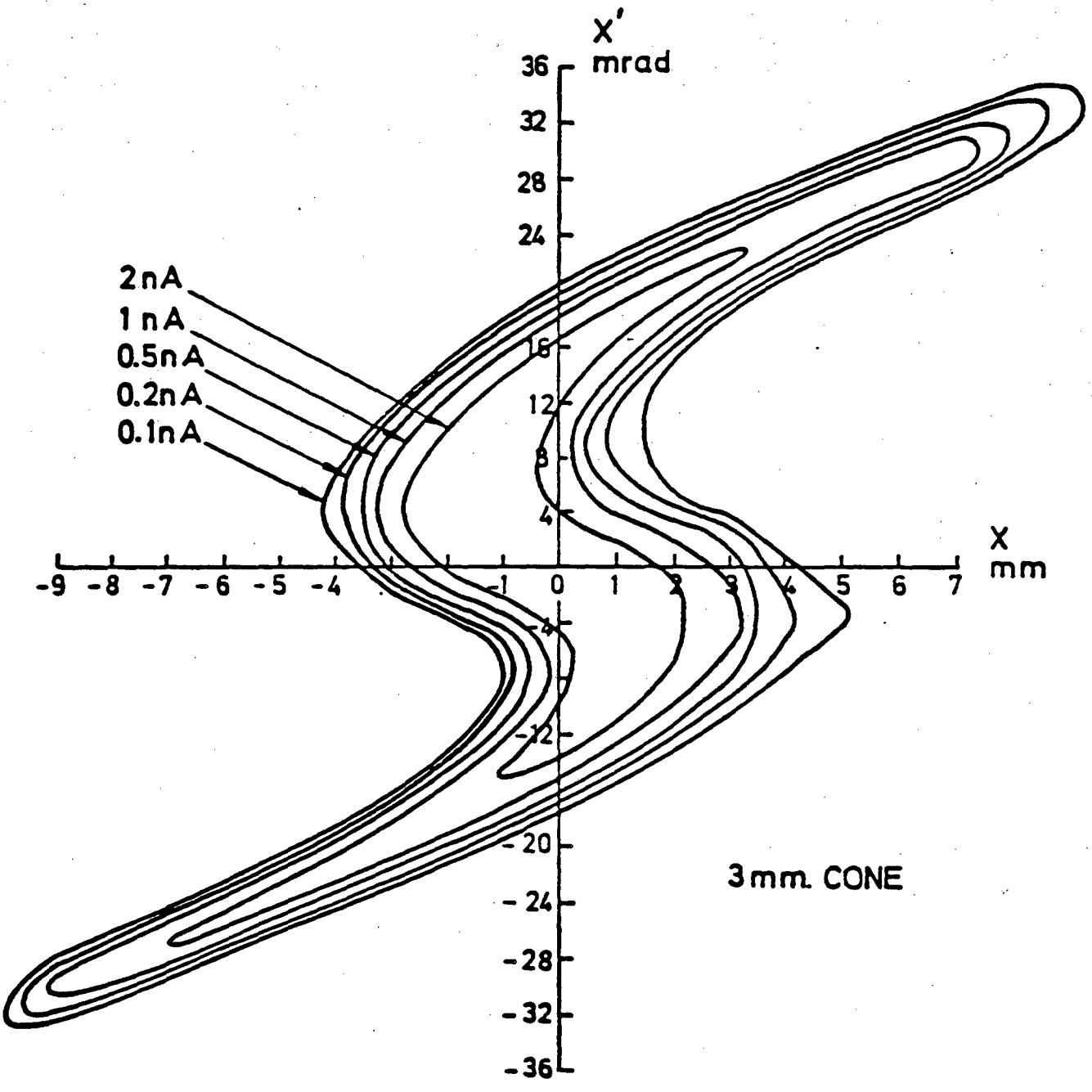

Figure 10.

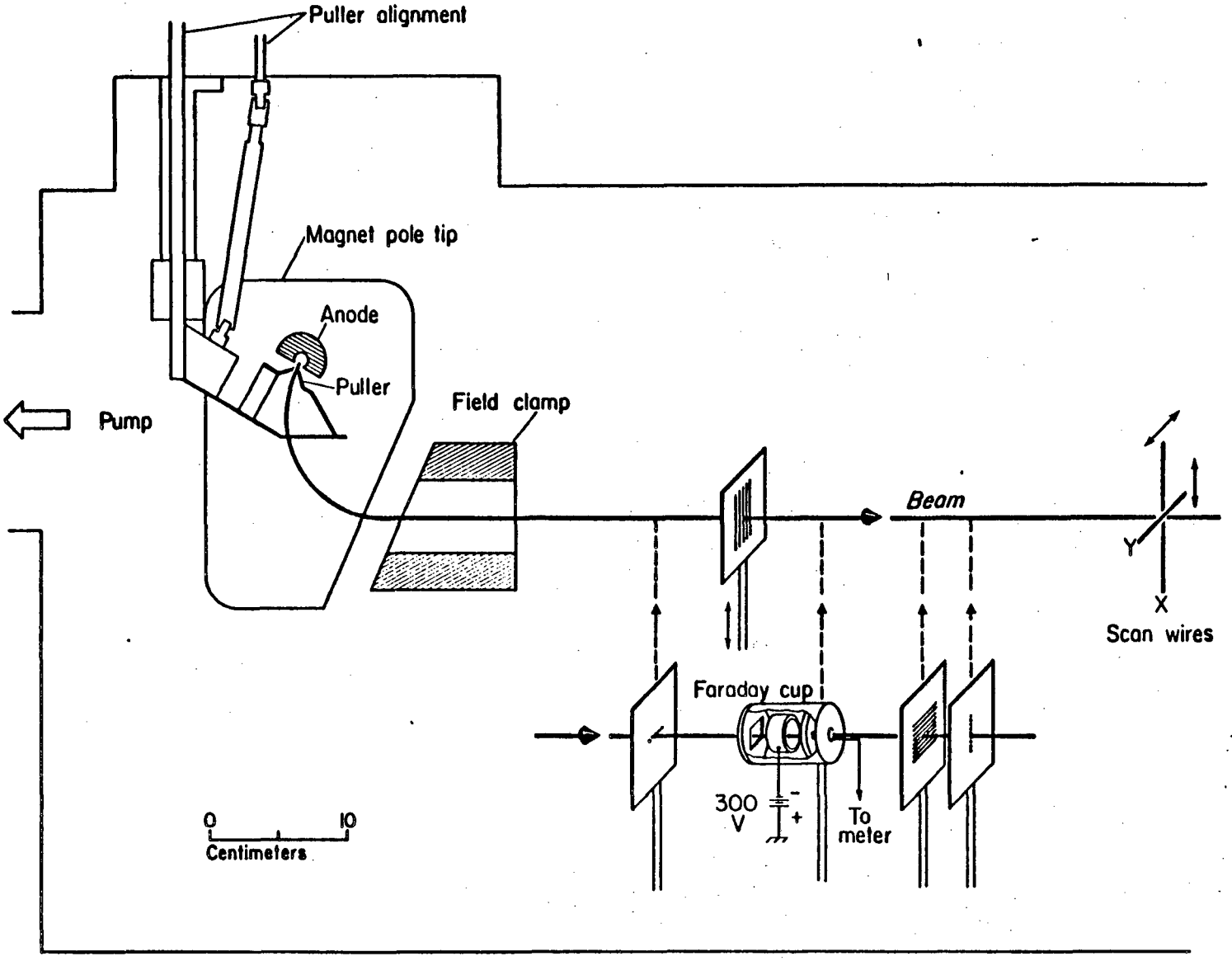

Figure 11.

EMITTANCE MEASUREMENTS FOR 60 μA D.C. BEAM CURRENT OF Ar^{5+} AT 10 kV EXTRACTION VOLTAGE

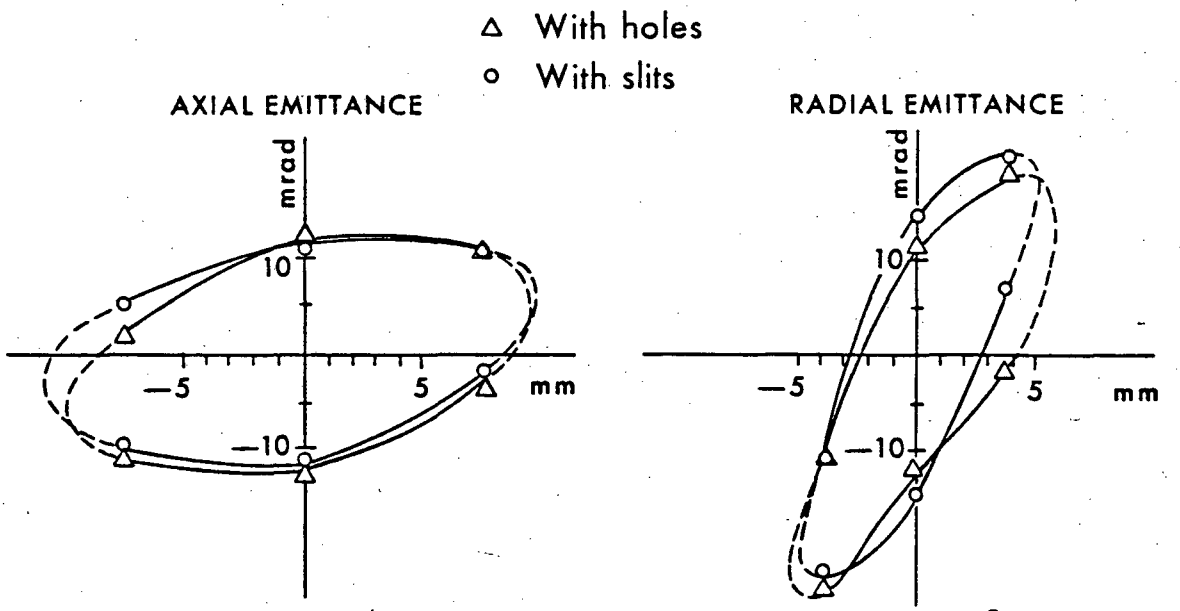

$E_{\Delta} = 1.11\,\pi \cdot 10^{-4}$ m·rad
$E_{o} = 1.16\,\pi \cdot 10^{-4}$ m·rad

$E_{\Delta} = 7.1\,\pi \cdot 10^{-5}$ m·rad
$E_{o} = 6.9\,\pi \cdot 10^{-5}$ m·rad

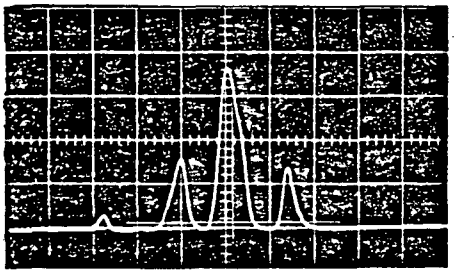

Axial emittance with slits, 20 ms/div

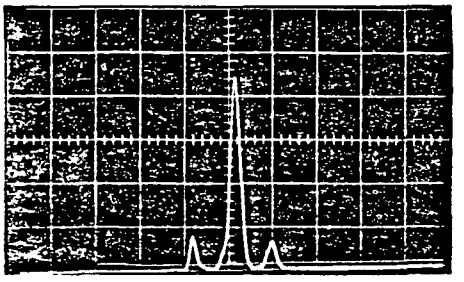

Radial emittance with slits, 20 ms/div

Figure 12.

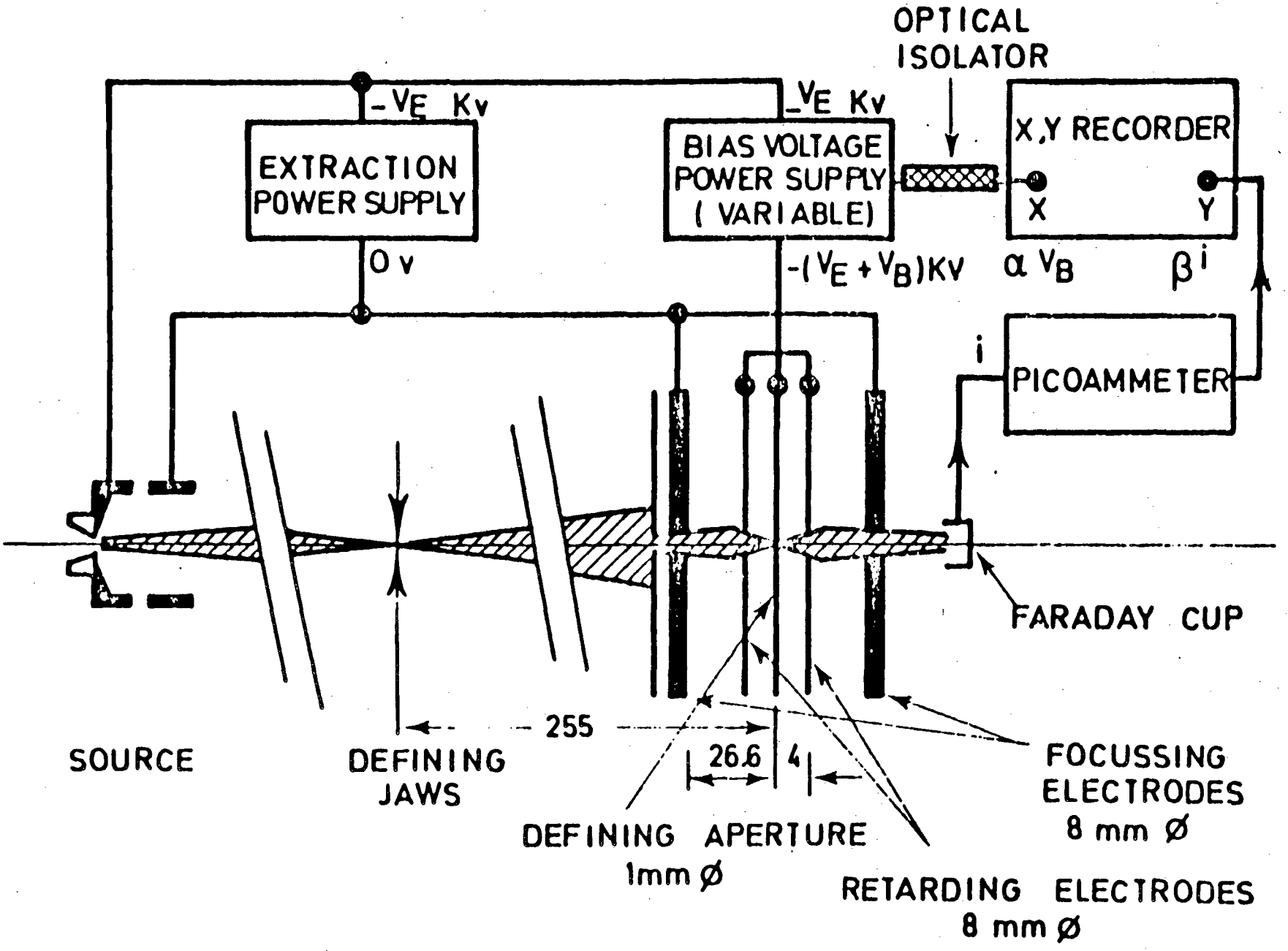

Figure 13.

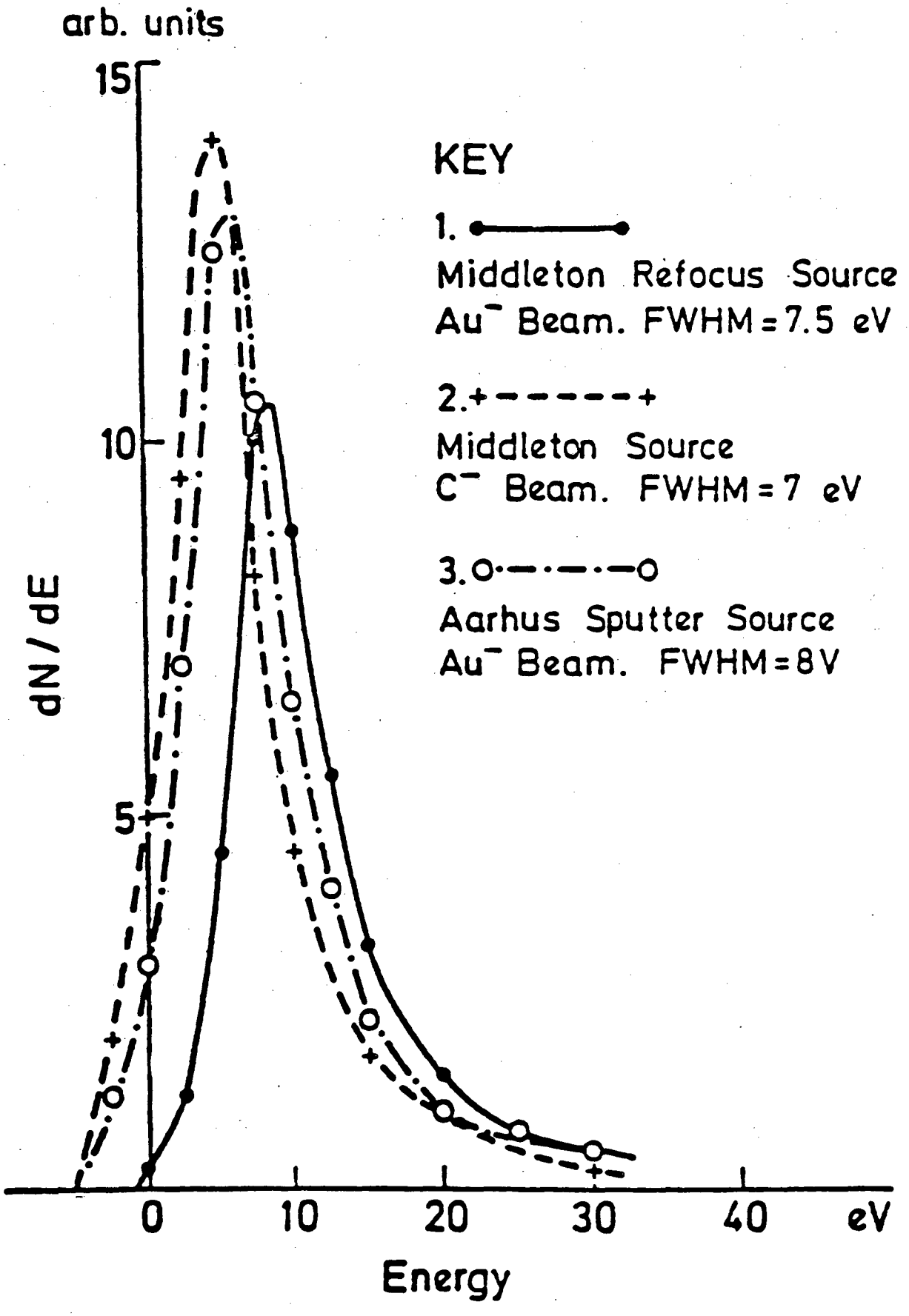

Figure 14.

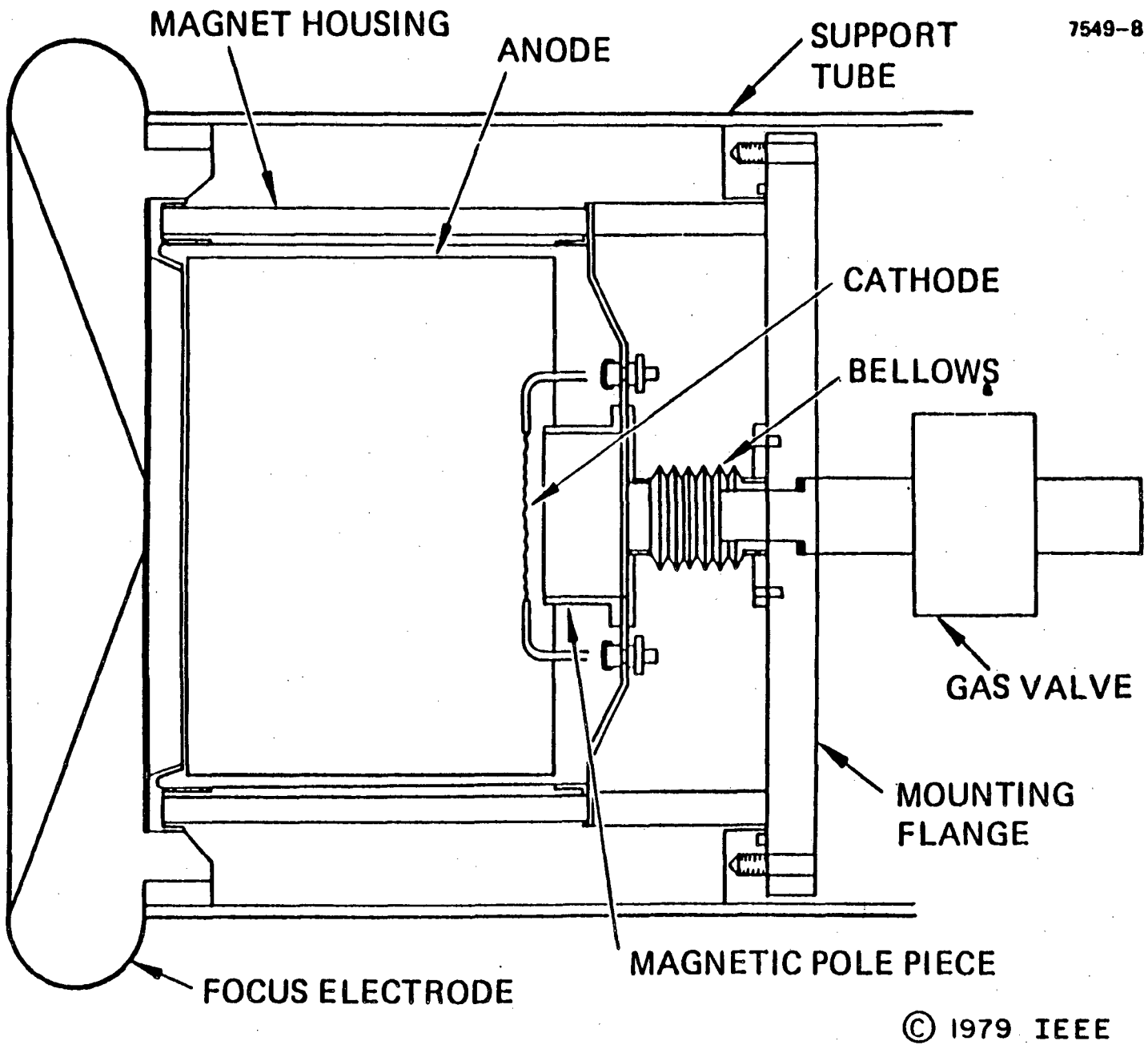
MAGNET HOUSING
ANODE
SUPPORT TUBE
7549-8
CATHODE
BELLOWS
GAS VALVE
MOUNTING FLANGE
MAGNETIC POLE PIECE
FOCUS ELECTRODE
© 1979 IEEE

Figure 15.

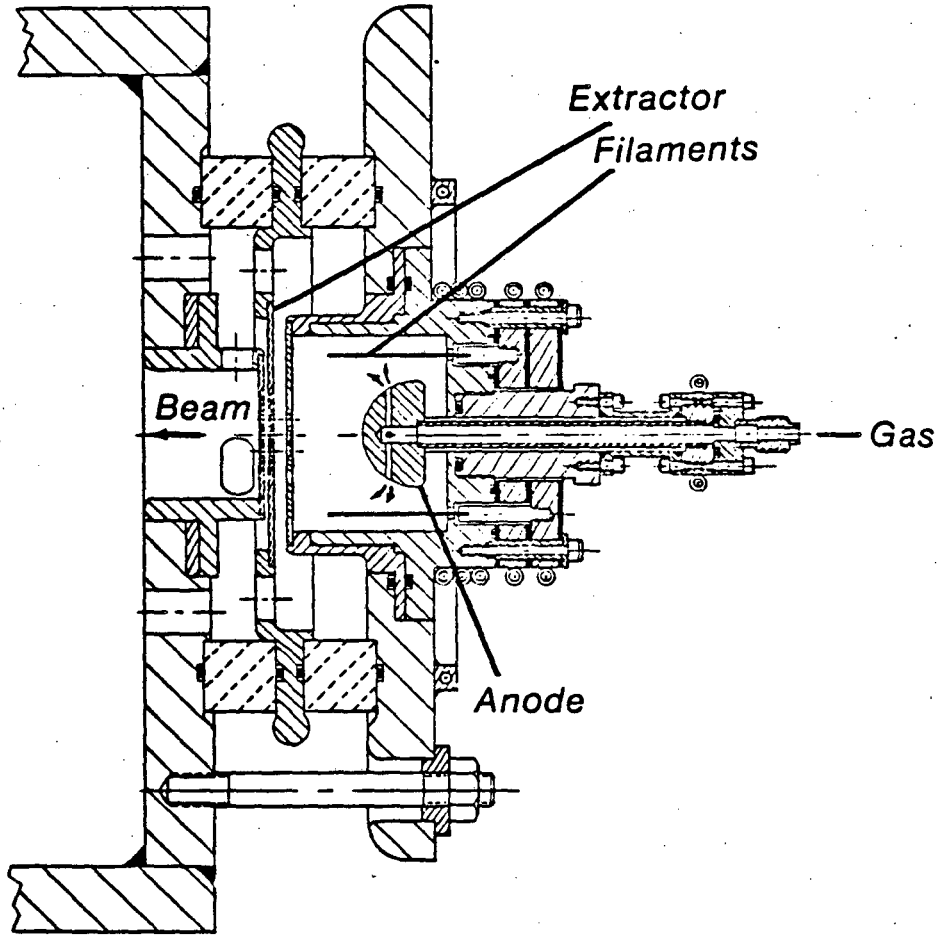

XBL 793-8705

Figure 16.

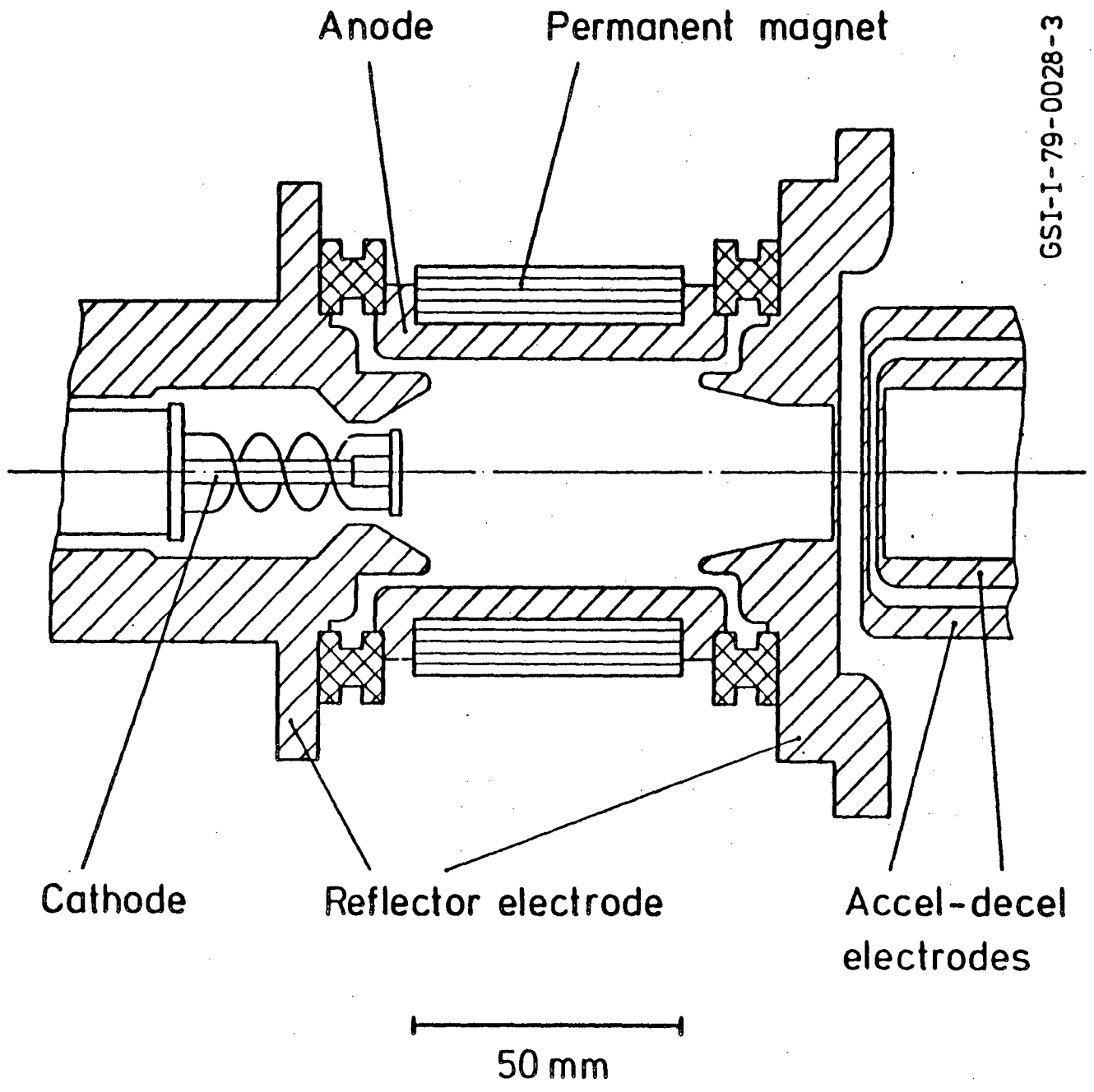
Anode
Permanent magnet
GSI-I-79-0028-3
Cathode
Reflector electrode
Accel-decel
electrodes
50 mm

Figure 17.

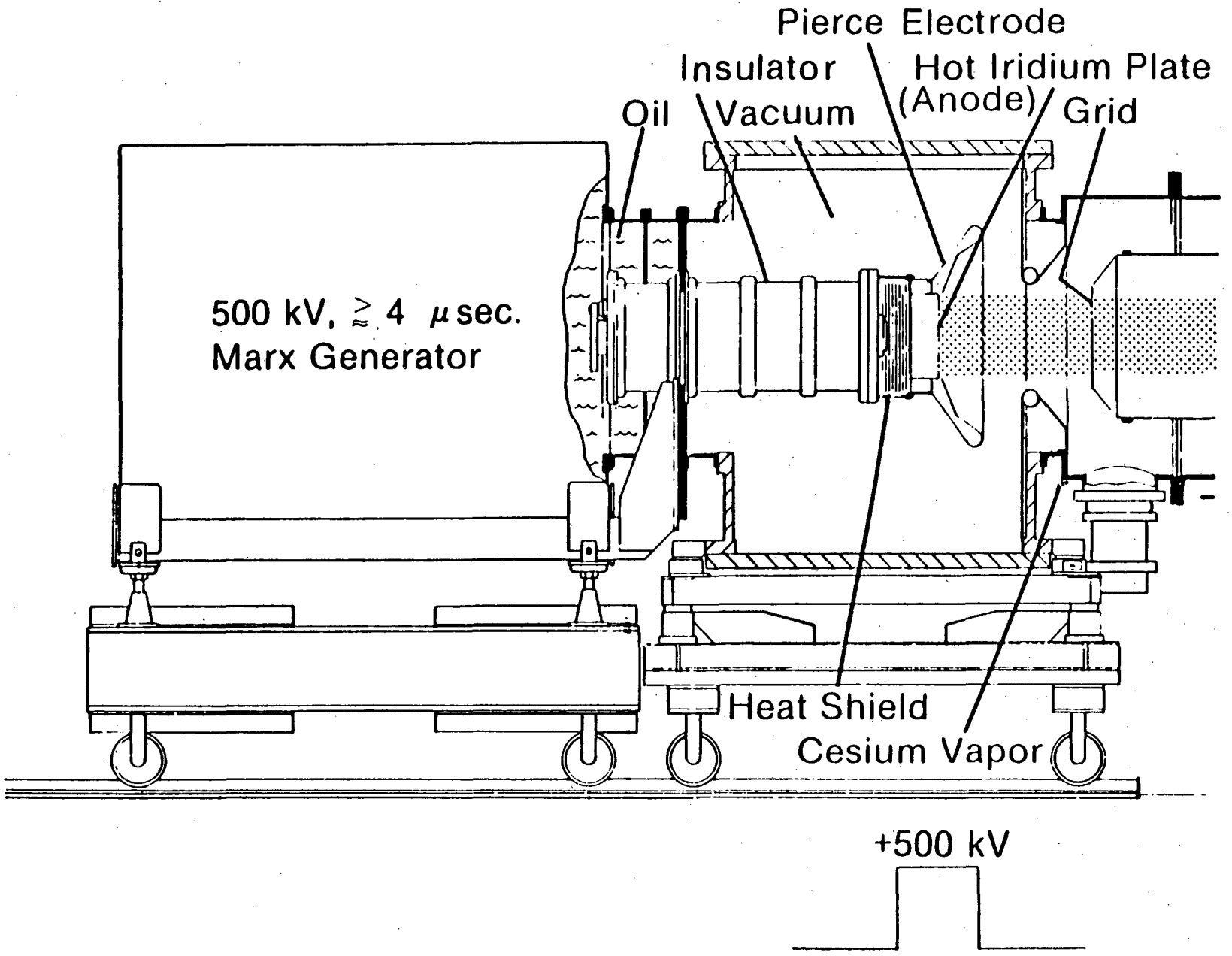

XBL 795-9591A

Figure 18.

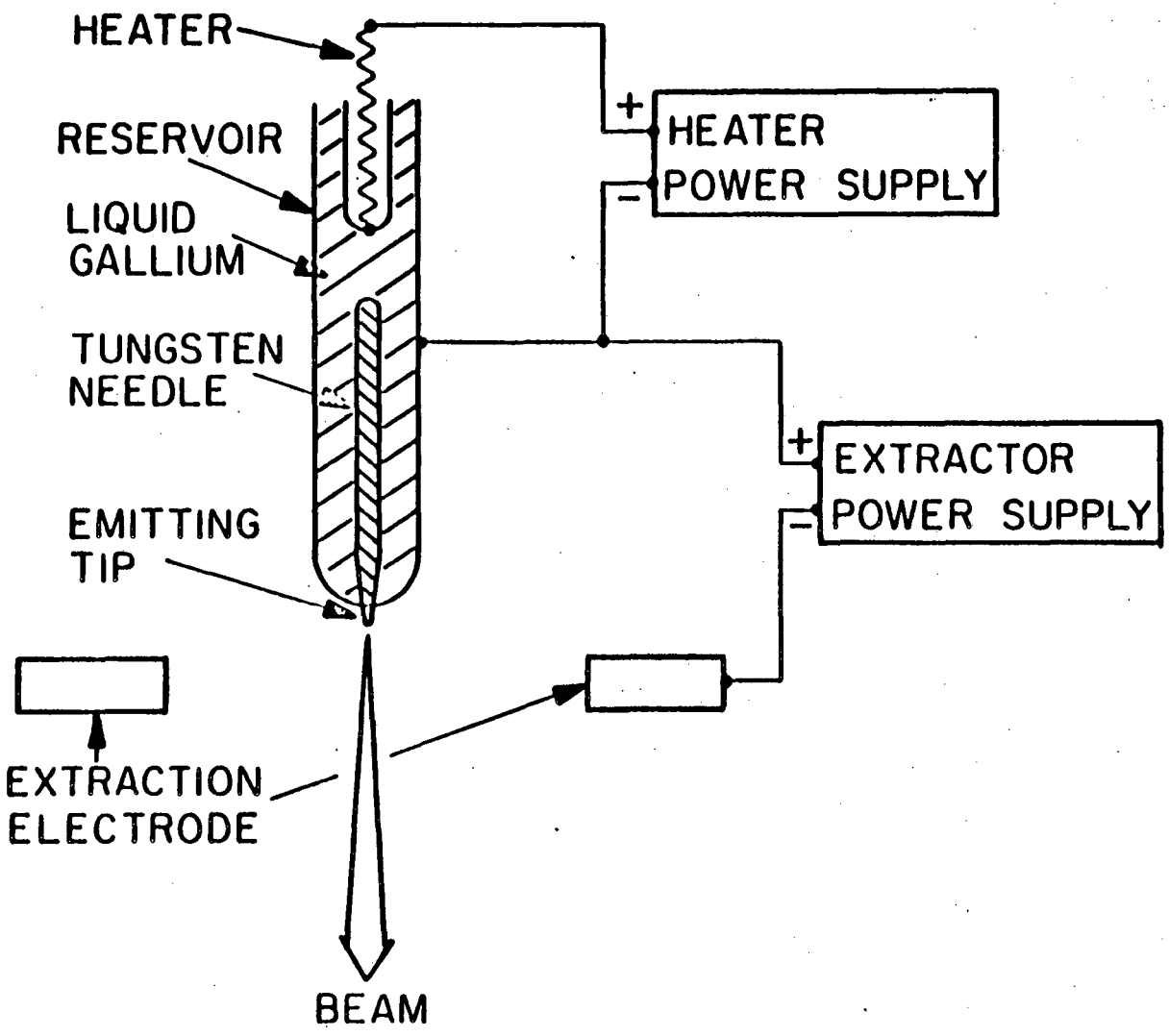
HEATER
RESERVOIR
LIQUID
GALLIUM
TUNGSTEN
NEEDLE
EMITTING
TIP
EXTRACTION
ELECTRODE
BEAM
+
HEATER
POWER SUPPLY
−
+
EXTRACTOR
POWER SUPPLY
−

Figure 19.

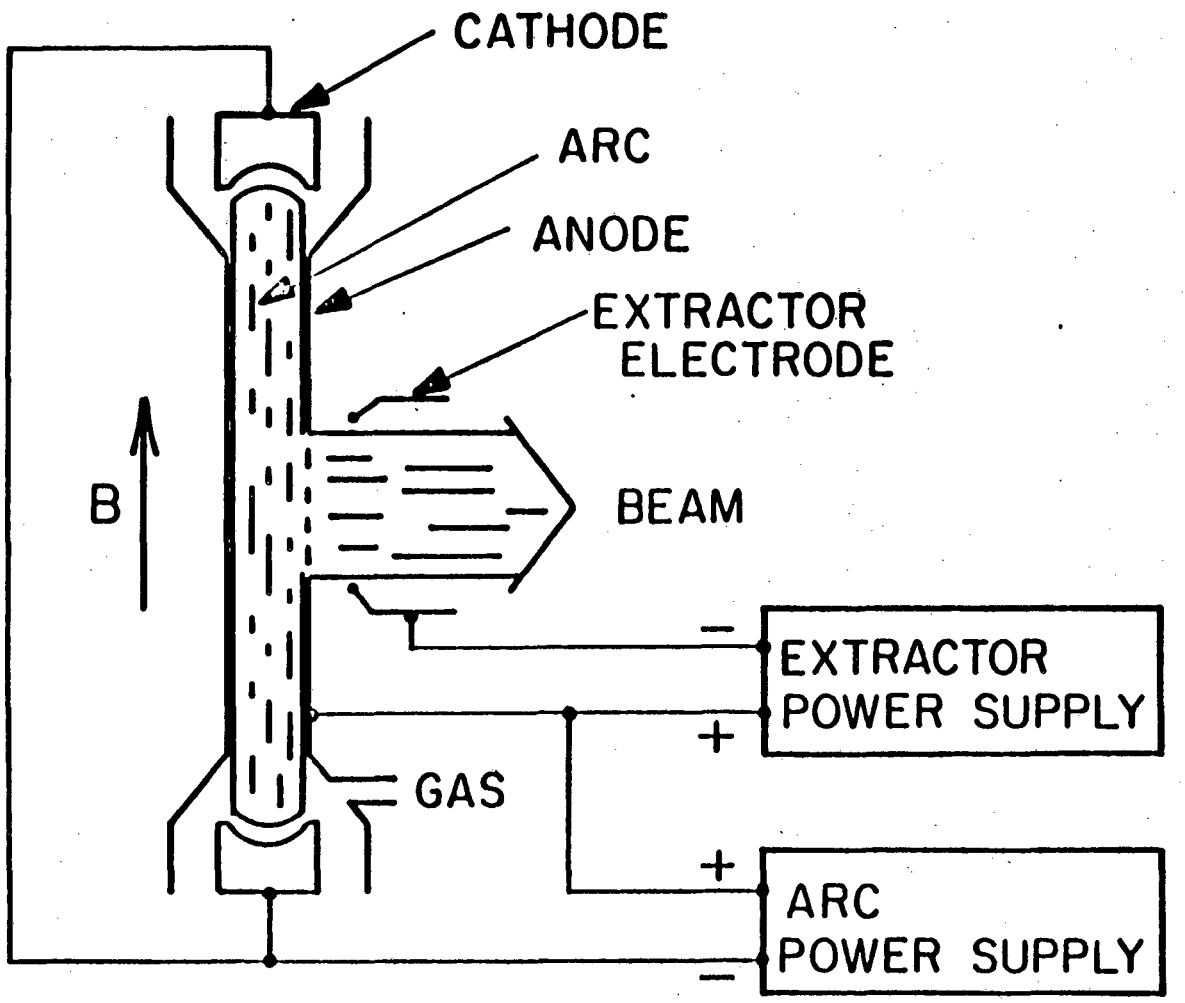
CATHODE
ARC
ANODE
EXTRACTOR
ELECTRODE
B
BEAM
EXTRACTOR
POWER SUPPLY
GAS
ARC
POWER SUPPLY

Figure 20.

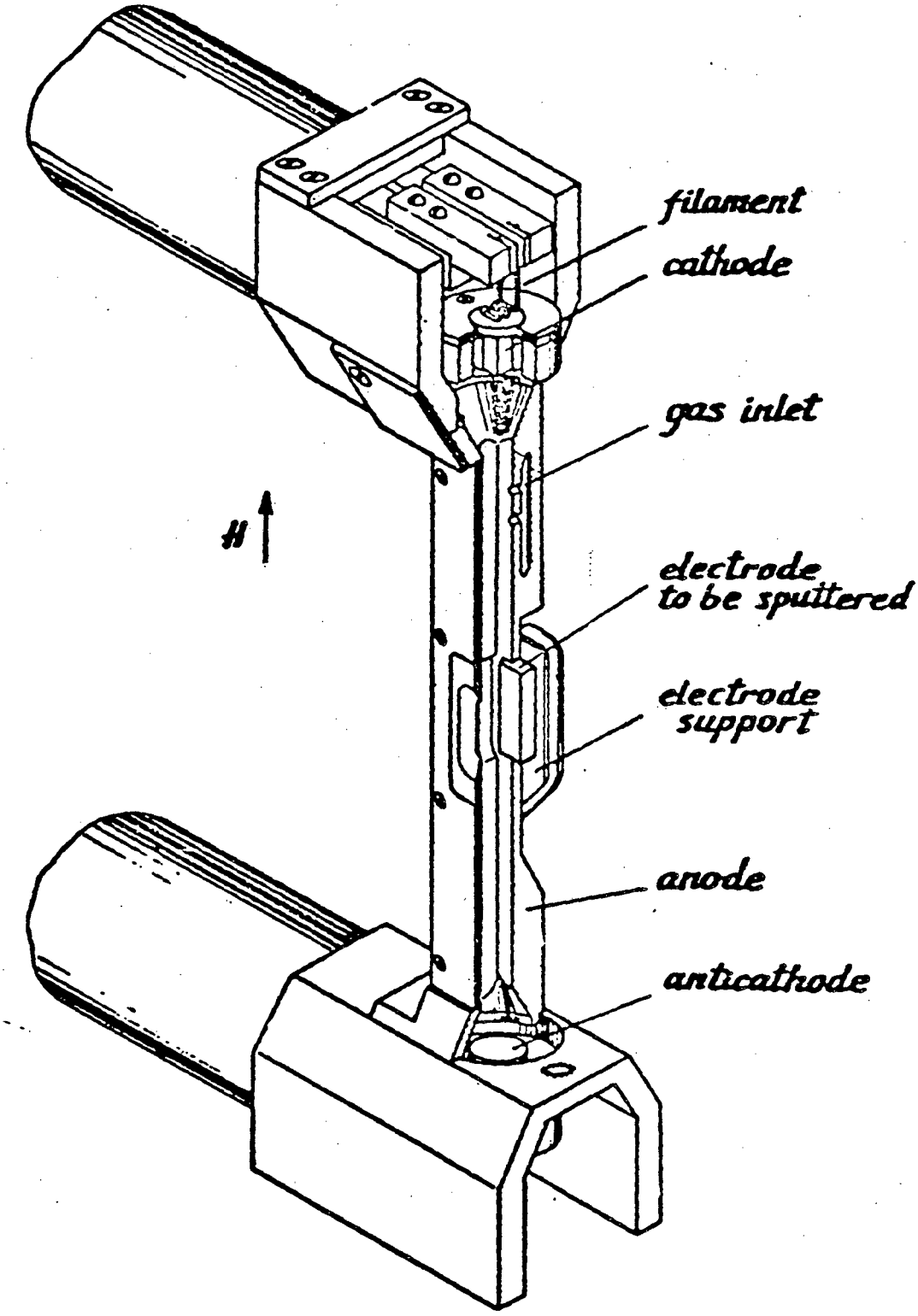
filament
cathode
gas inlet
H
electrode
to be sputtered
electrode
support
anode
anticathode
XBL 772-7789

Figure 21.

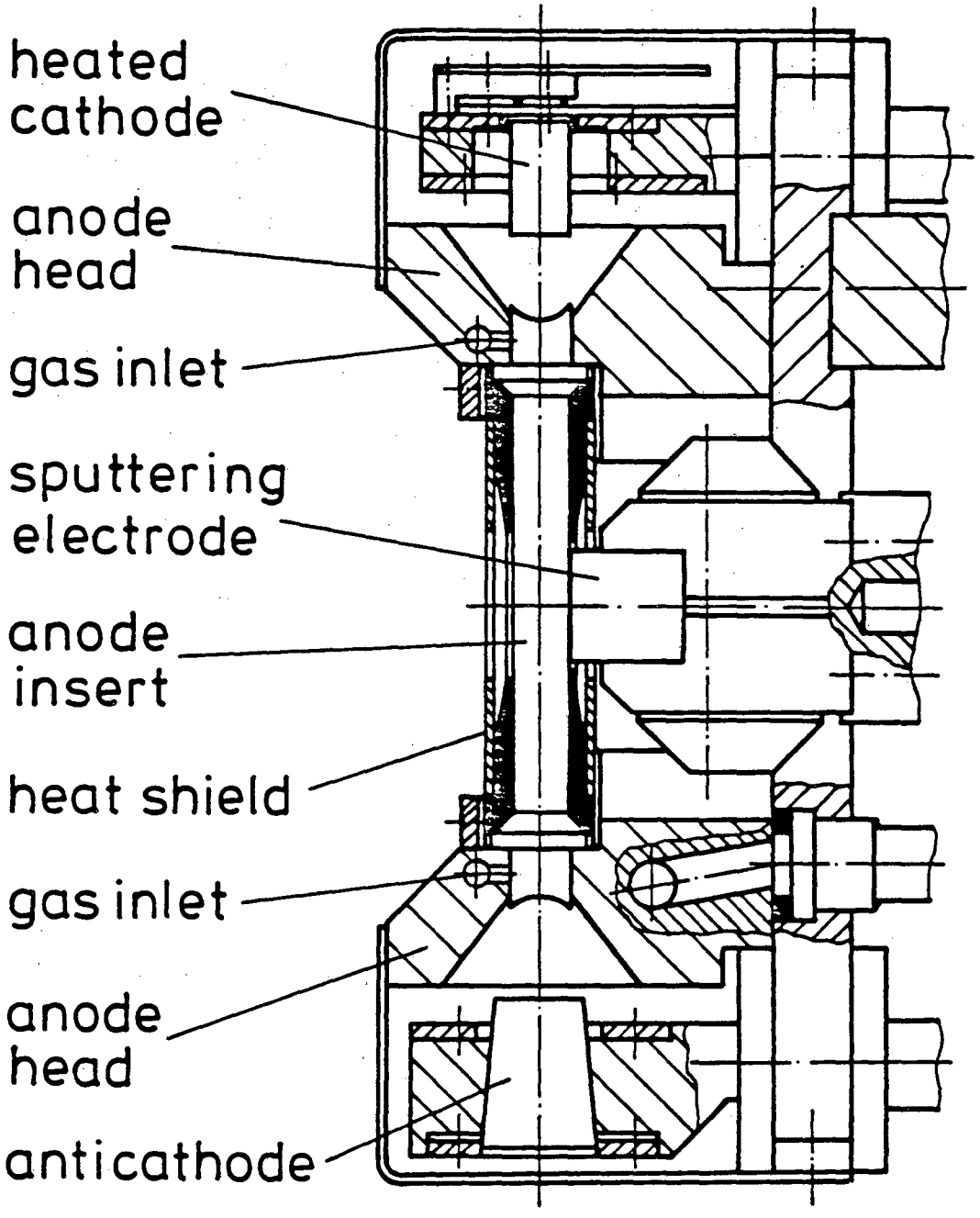

Figure 22.

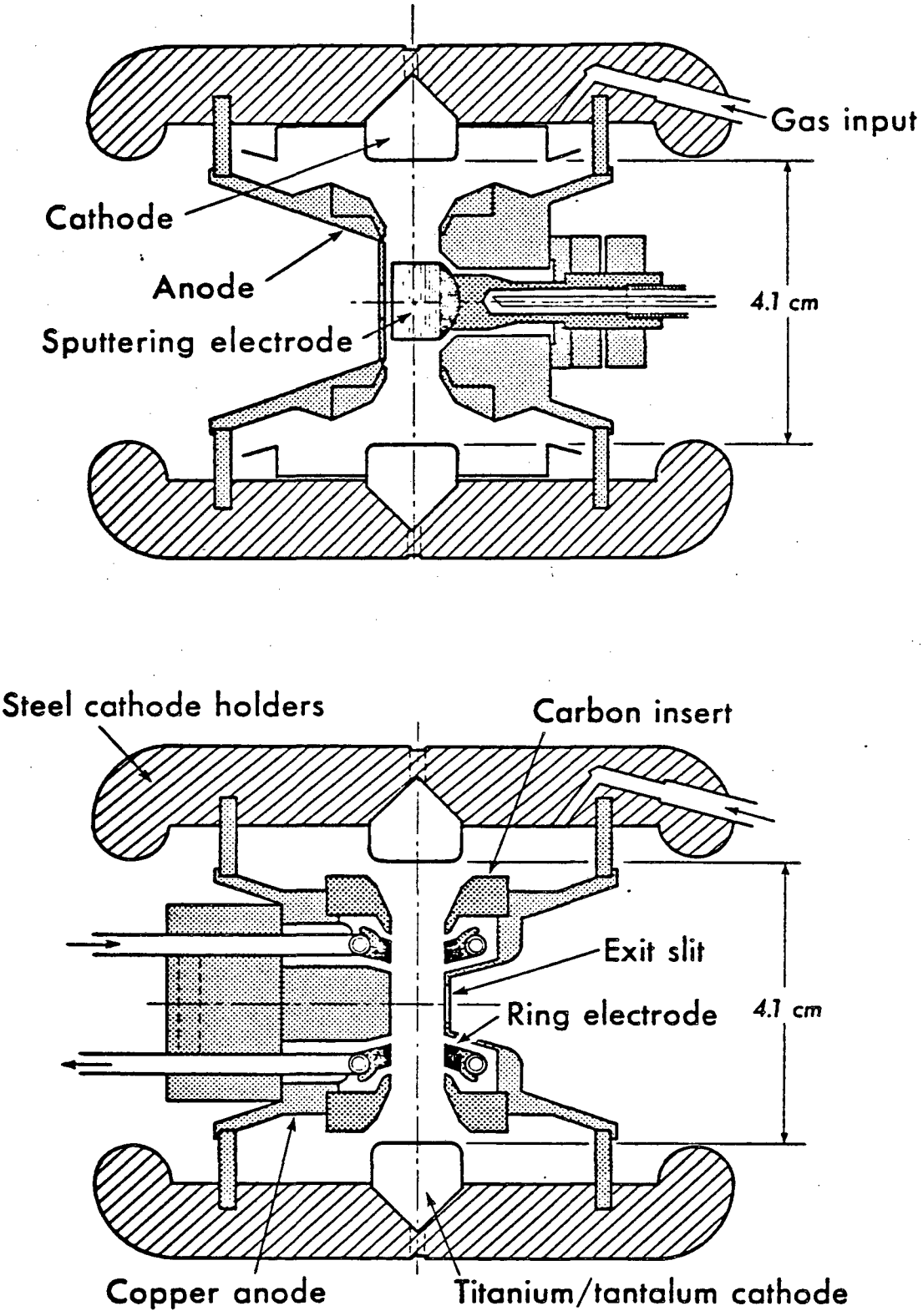

XBL 7510-4167 a

Figure 23.

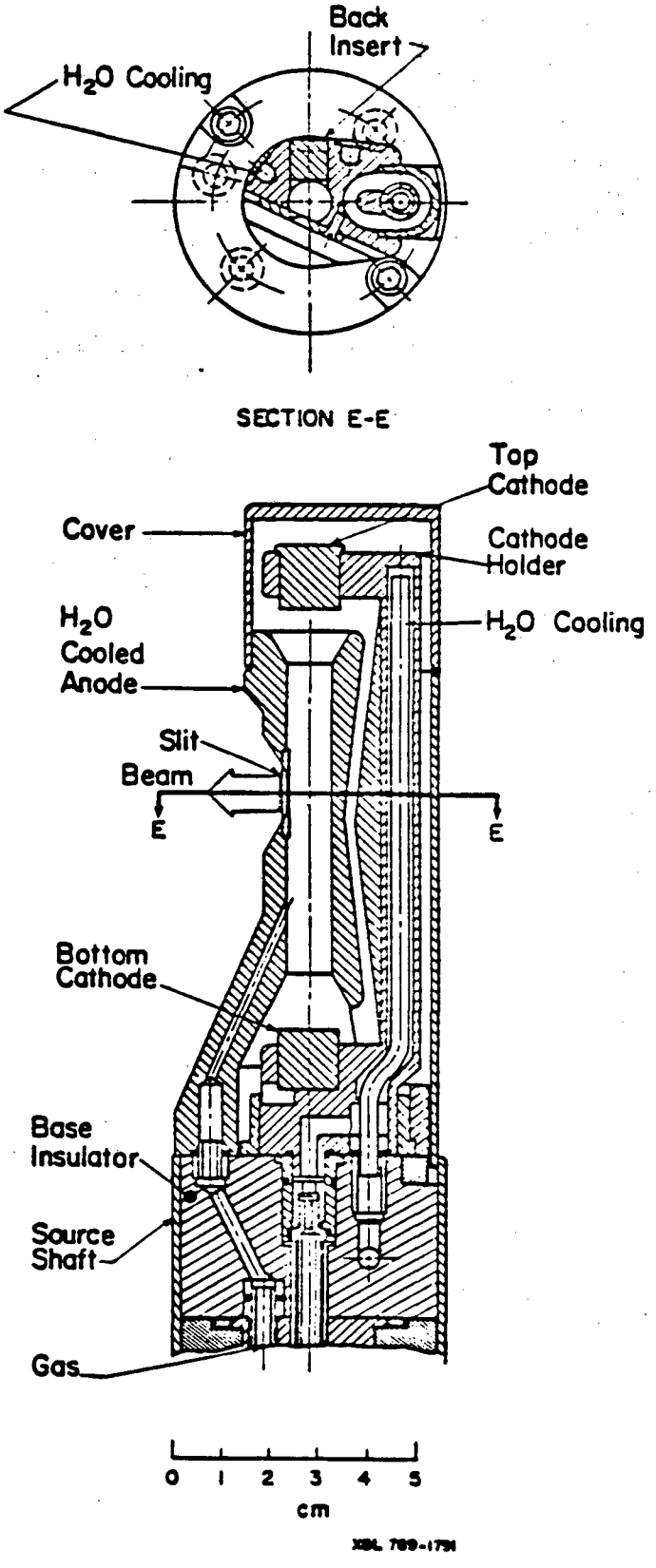

Figure 24.

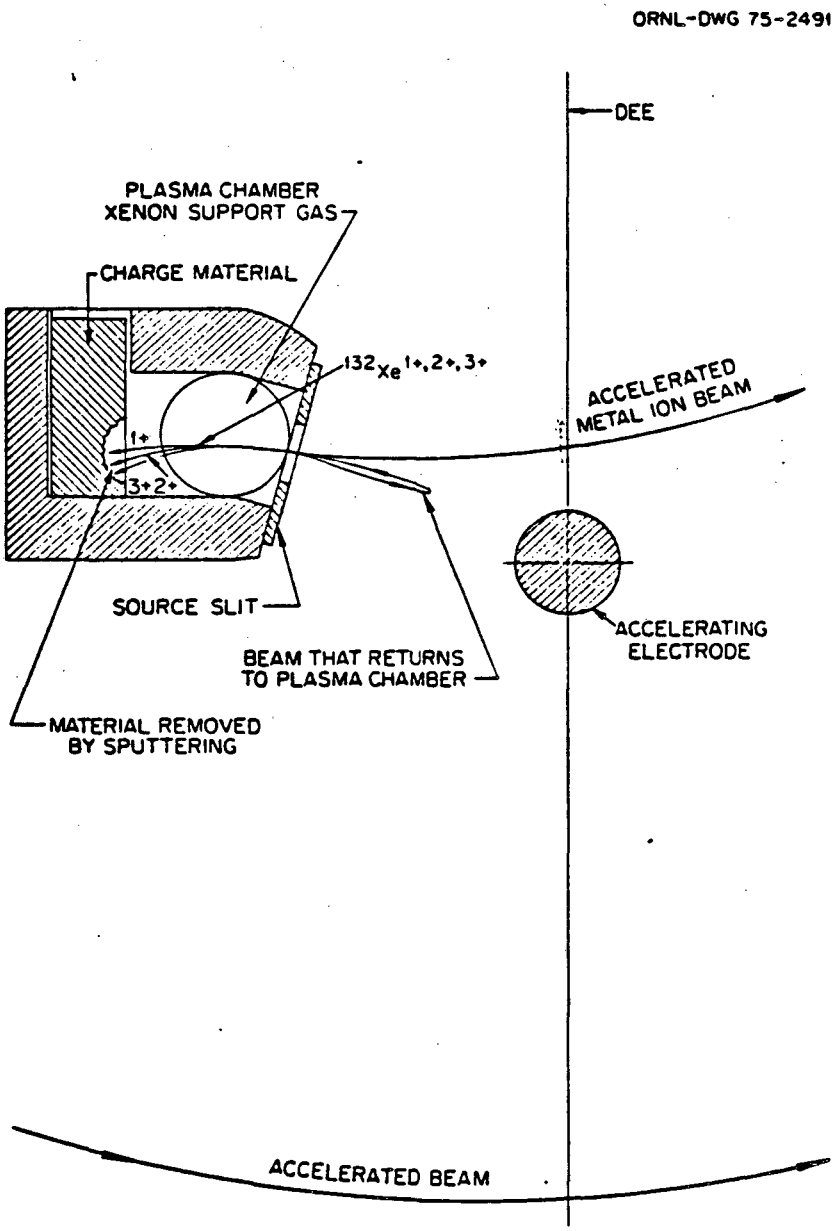

Cyclotron Median Plane View of Metal Ion Source.

Figure 25.

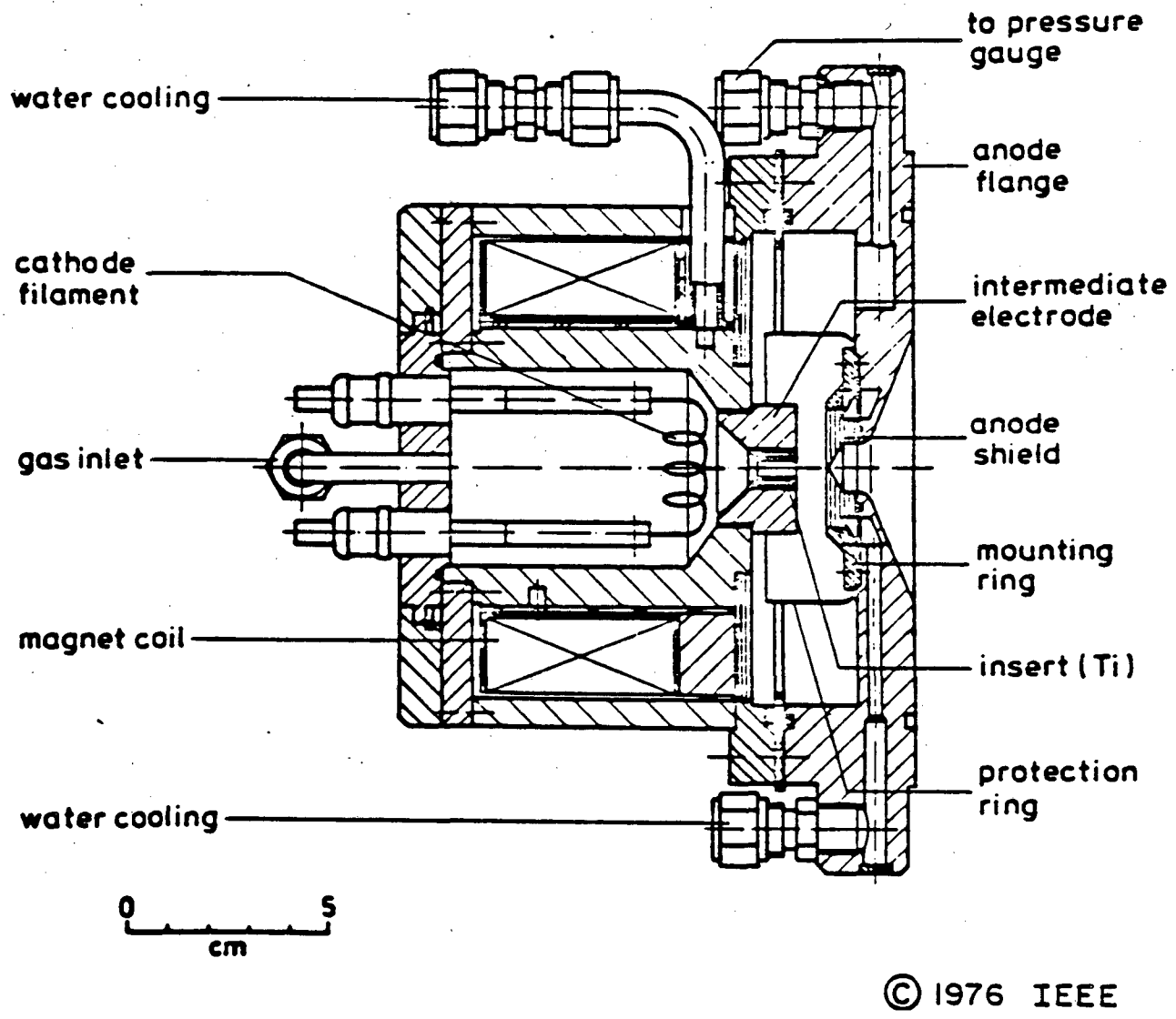

Figure 26.

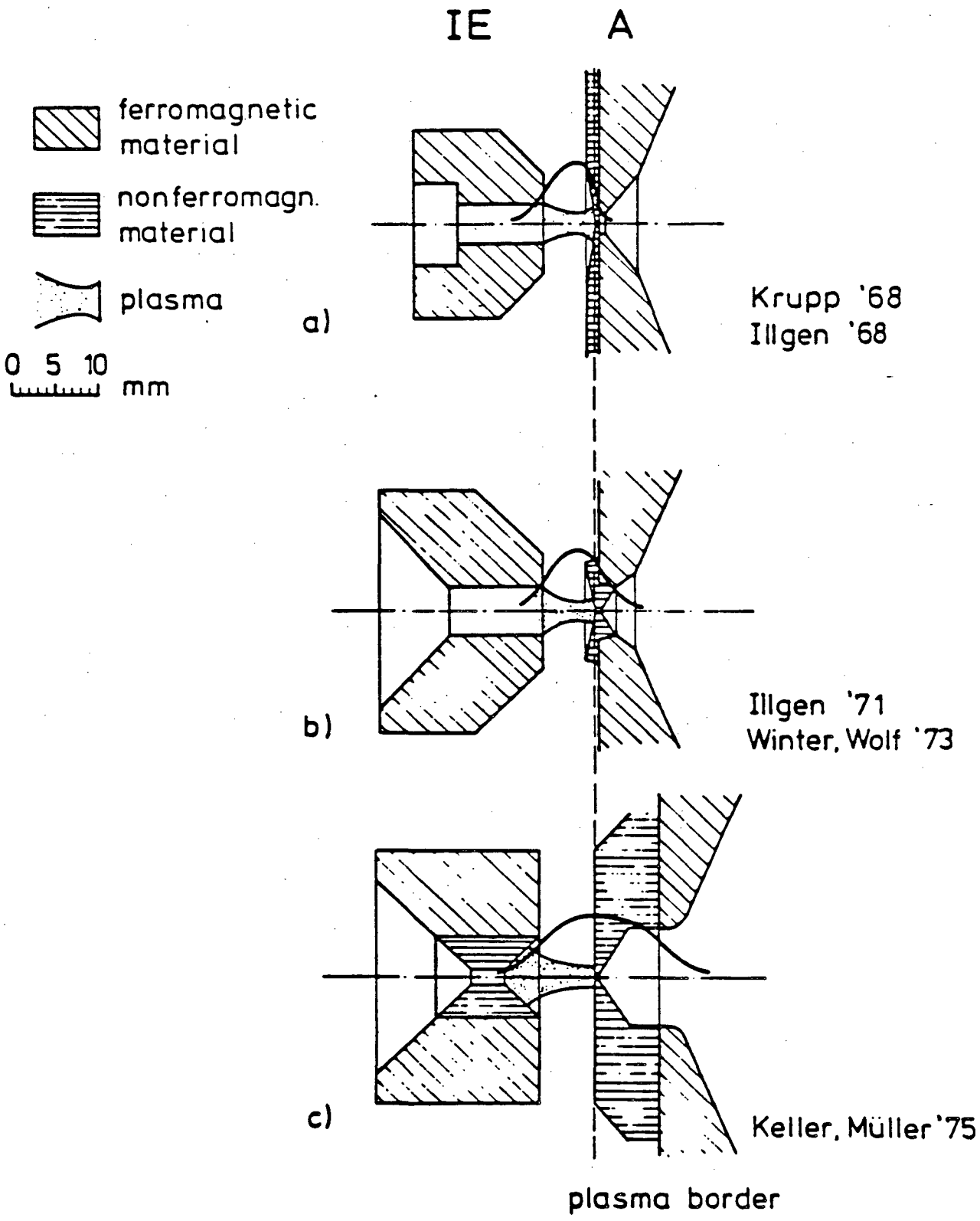

Figure 27.

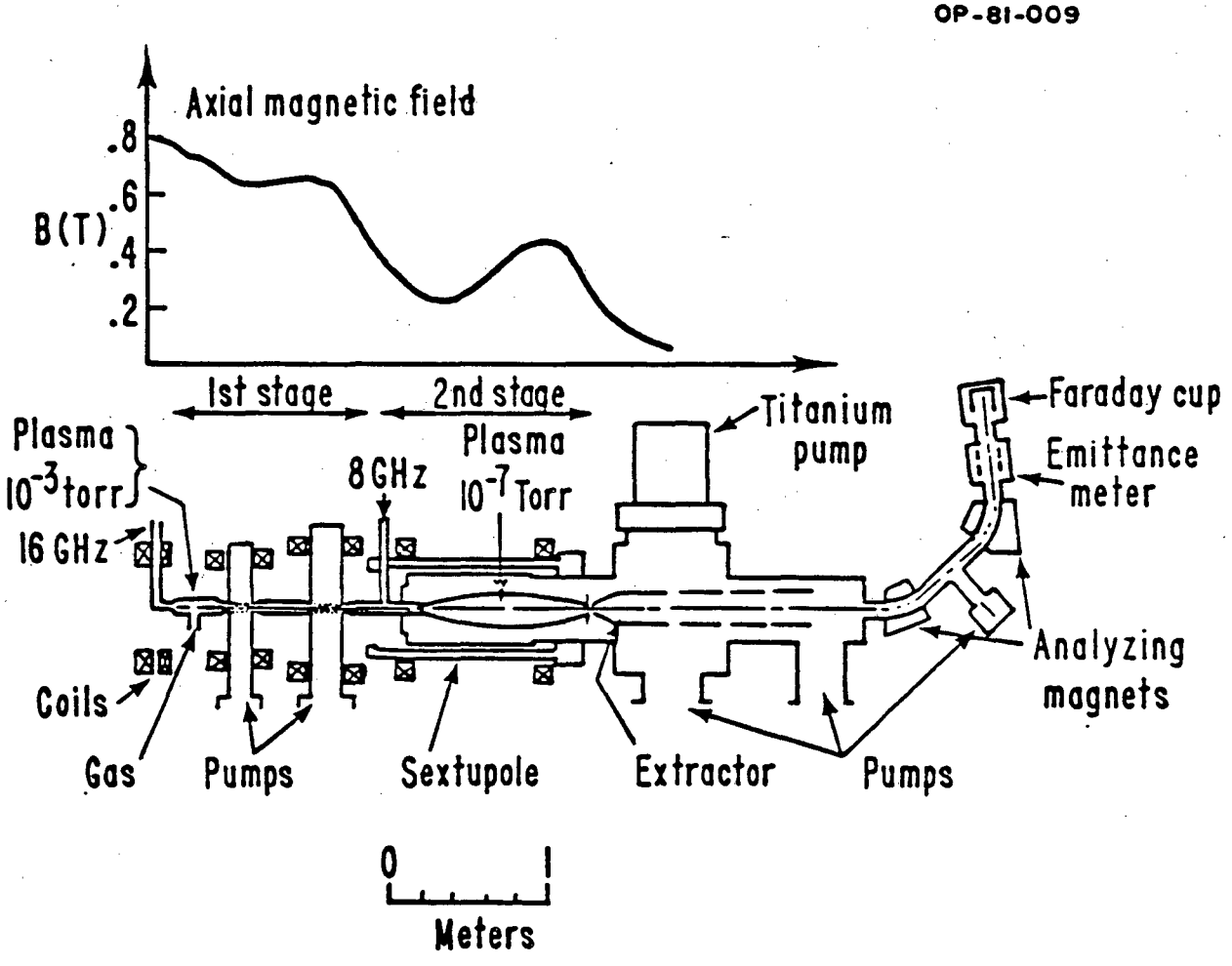
OP-81-009
Axial magnetic field
B(T)
.8
.6
.4
.2
1st stage
2nd stage
Plasma
10^{-3} torr
16 GHz
8 GHz
Plasma
10^{-7} Torr
Titanium pump
Faraday cup
Emittance meter
Analyzing magnets
Coils
Gas
Pumps
Sextupole
Extractor
Pumps
0
1
Meters
XBL 7812-13426

Figure 28.

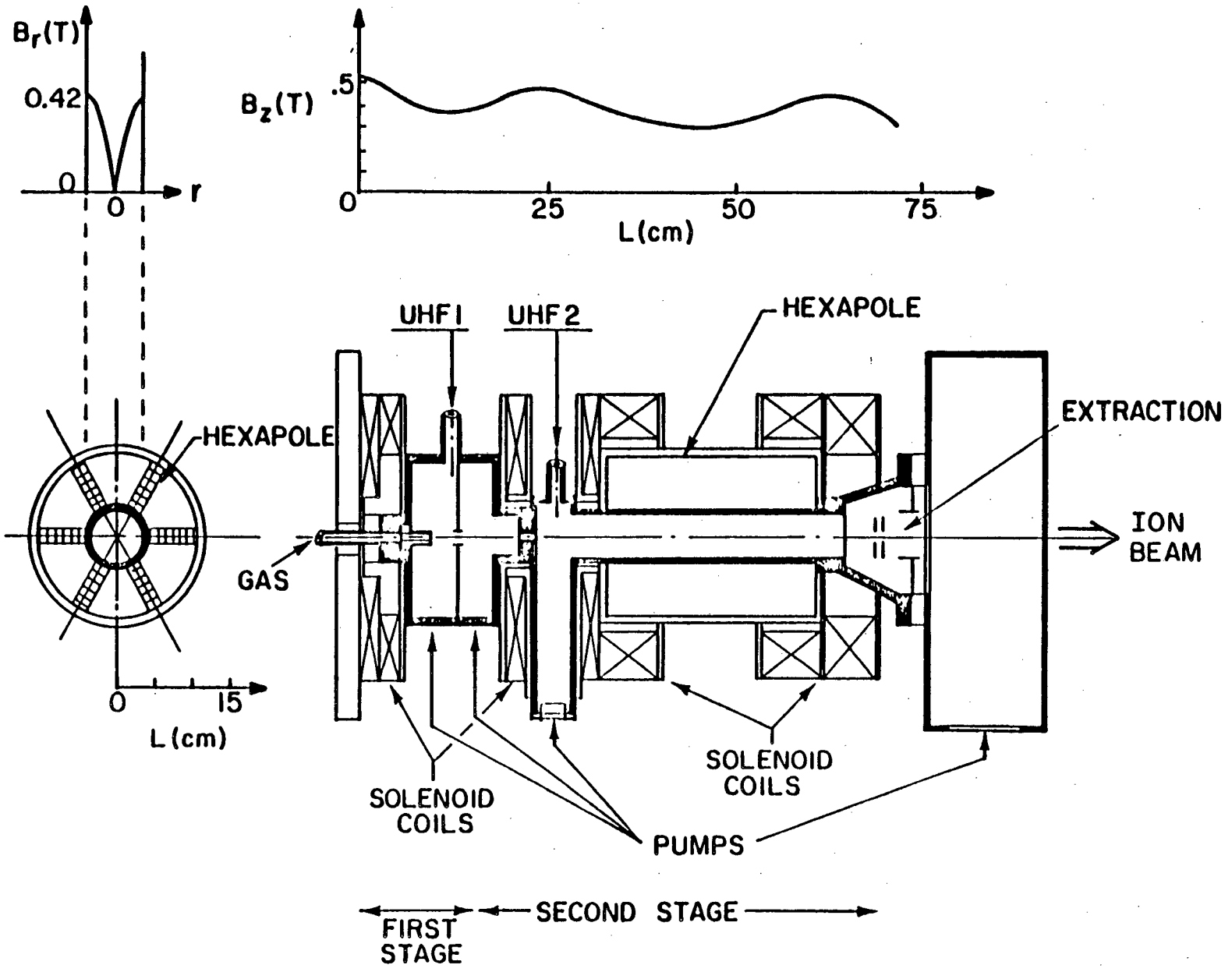
B_r(T)
0.42
0
r
0
B_z(T)
.5
0
25
50
75
L(cm)
UHF1
UHF2
HEXAPOLE
EXTRACTION
HEXAPOLE
GAS
ION
BEAM
0
15
L(cm)
SOLENOID
COILS
SOLENOID
COILS
PUMPS
FIRST
STAGE
SECOND STAGE

Figure 29.

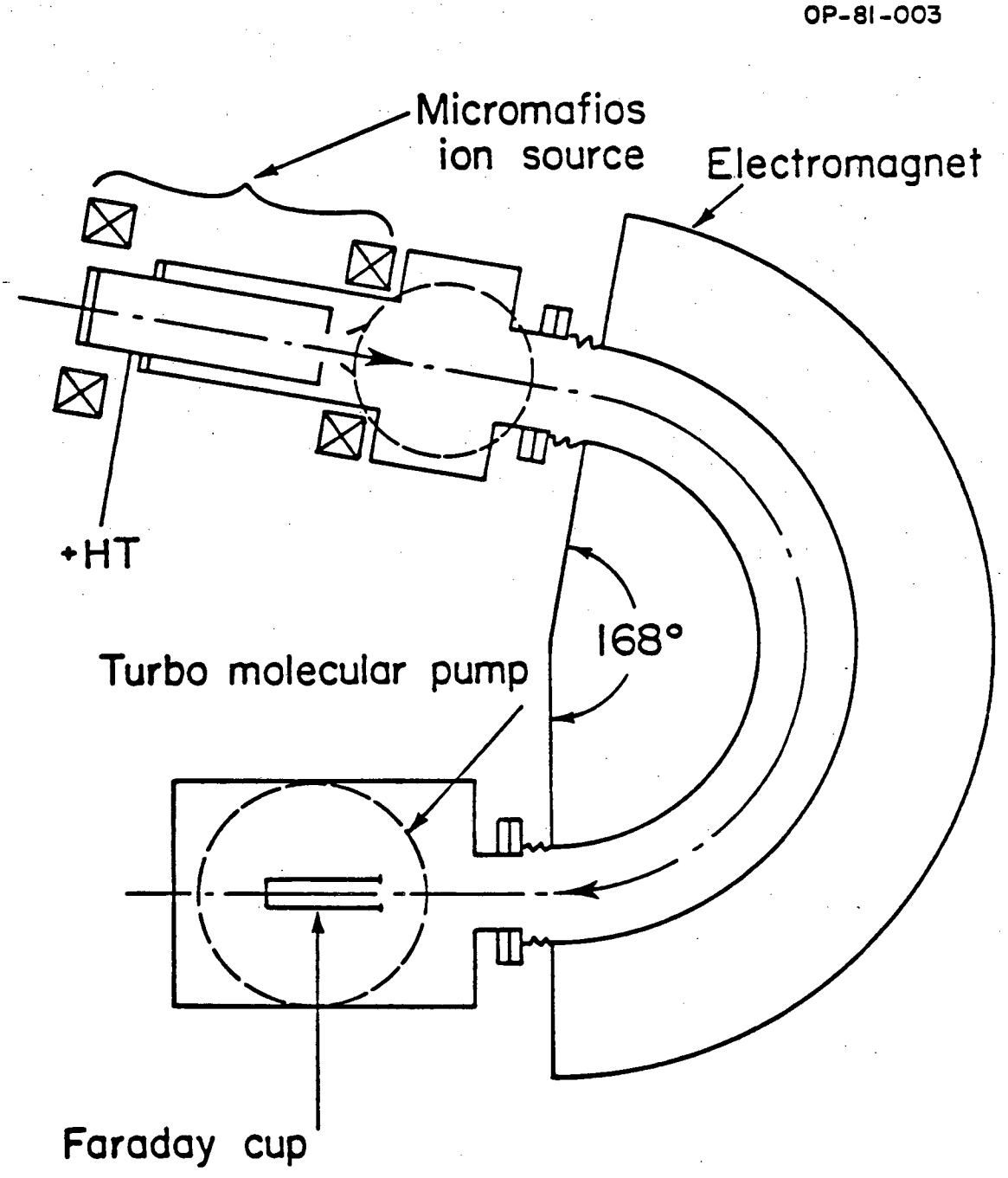
OP-81-003
Micromafios
ion source
Electromagnet
+HT
168°
Turbo molecular pump
Faraday cup

Figure 30.

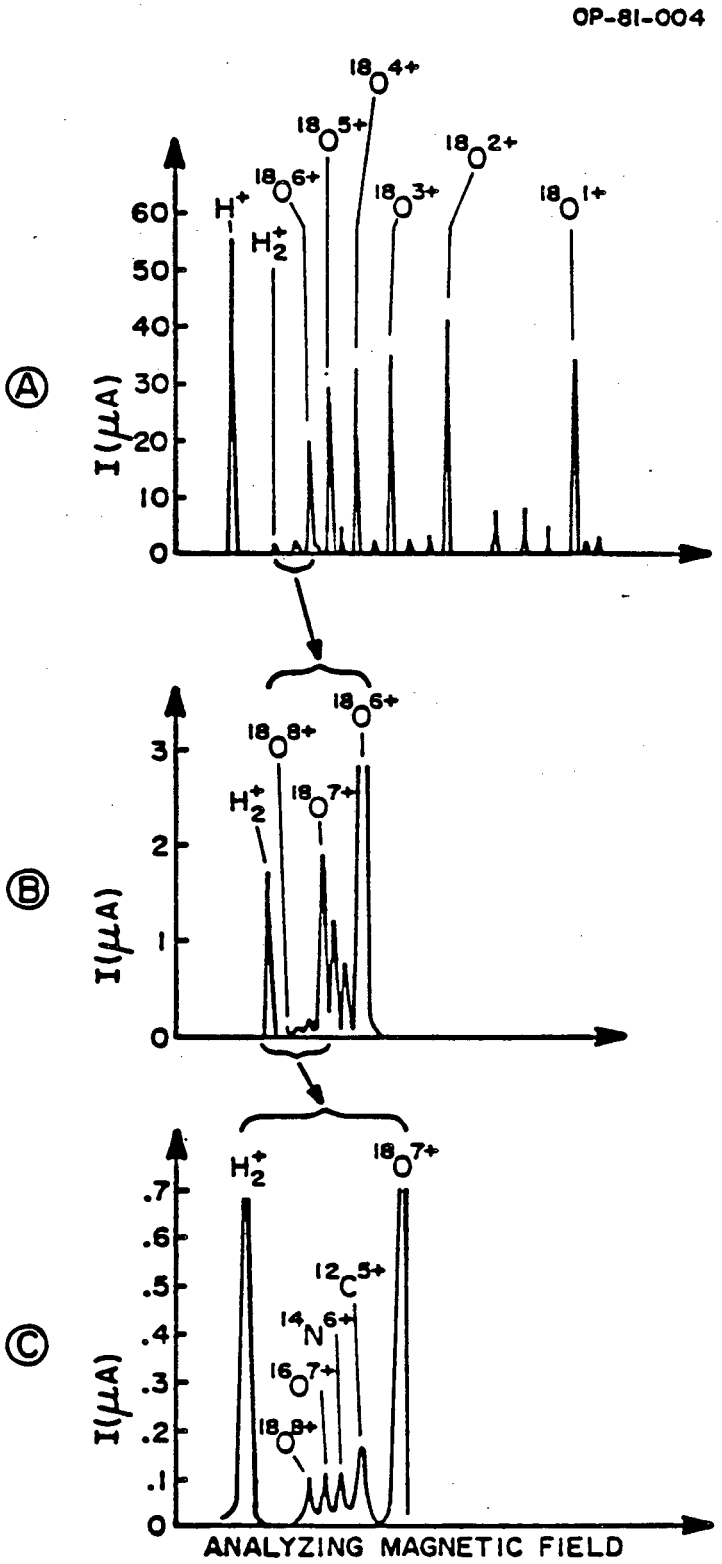
OP-81-004
Ⓐ
Ⓑ
Ⓒ
I(μA)
$^{18}O^{4+}$
$^{18}O^{5+}$
$^{18}O^{2+}$
$^{18}O^{6+}$
$^{18}O^{3+}$
$^{18}O^{1+}$
H^+
H_2^+
$^{18}O^{8+}$
$^{18}O^{7+}$
$^{12}C^{5+}$
$^{14}N^{6+}$
$^{16}O^{7+}$
$^{18}O^{8+}$
ANALYZING MAGNETIC FIELD

Figure 31.

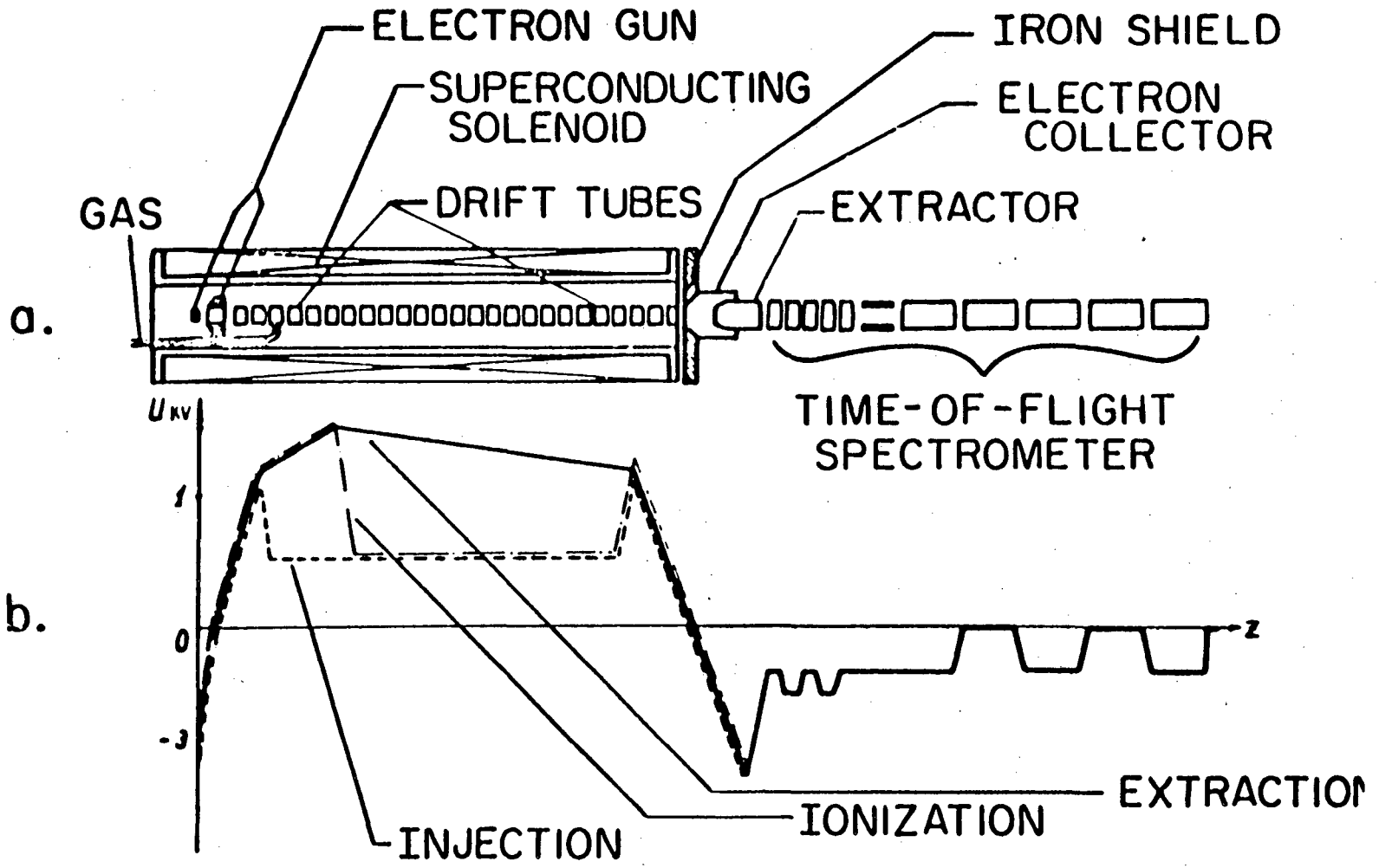
ELECTRON GUN
IRON SHIELD
SUPERCONDUCTING SOLENOID
ELECTRON COLLECTOR
GAS
DRIFT TUBES
EXTRACTOR
a.
TIME-OF-FLIGHT SPECTROMETER
U KV
1
0
-3
z
b.
EXTRACTION
IONIZATION
INJECTION

Figure 32.

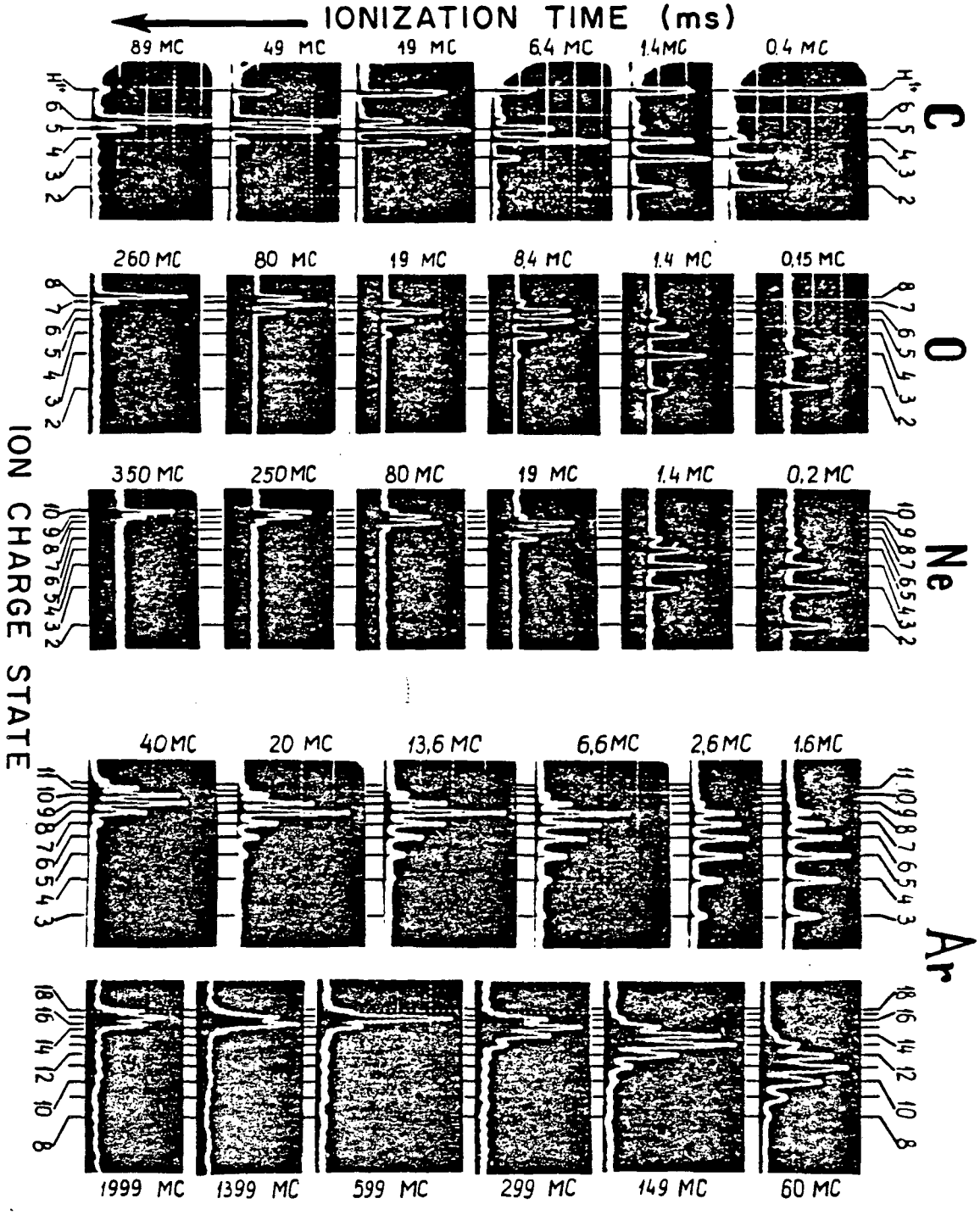
IONIZATION TIME (ms)
89 MC
49 MC
19 MC
6.4 MC
1.4MC
0.4 MC
C
260 MC
80 MC
19 MC
8.4 MC
1.4 MC
0.15 MC
O
350 MC
250MC
80 MC
19 MC
1.4 MC
0.2 MC
Ne
40MC
20 MC
13,6 MC
6,6MC
2,6MC
1.6MC
Ar
1999 MC
1399 MC
599 MC
299 MC
149 MC
60 MC
ION CHARGE STATE

Figure 33.

OP-81-001

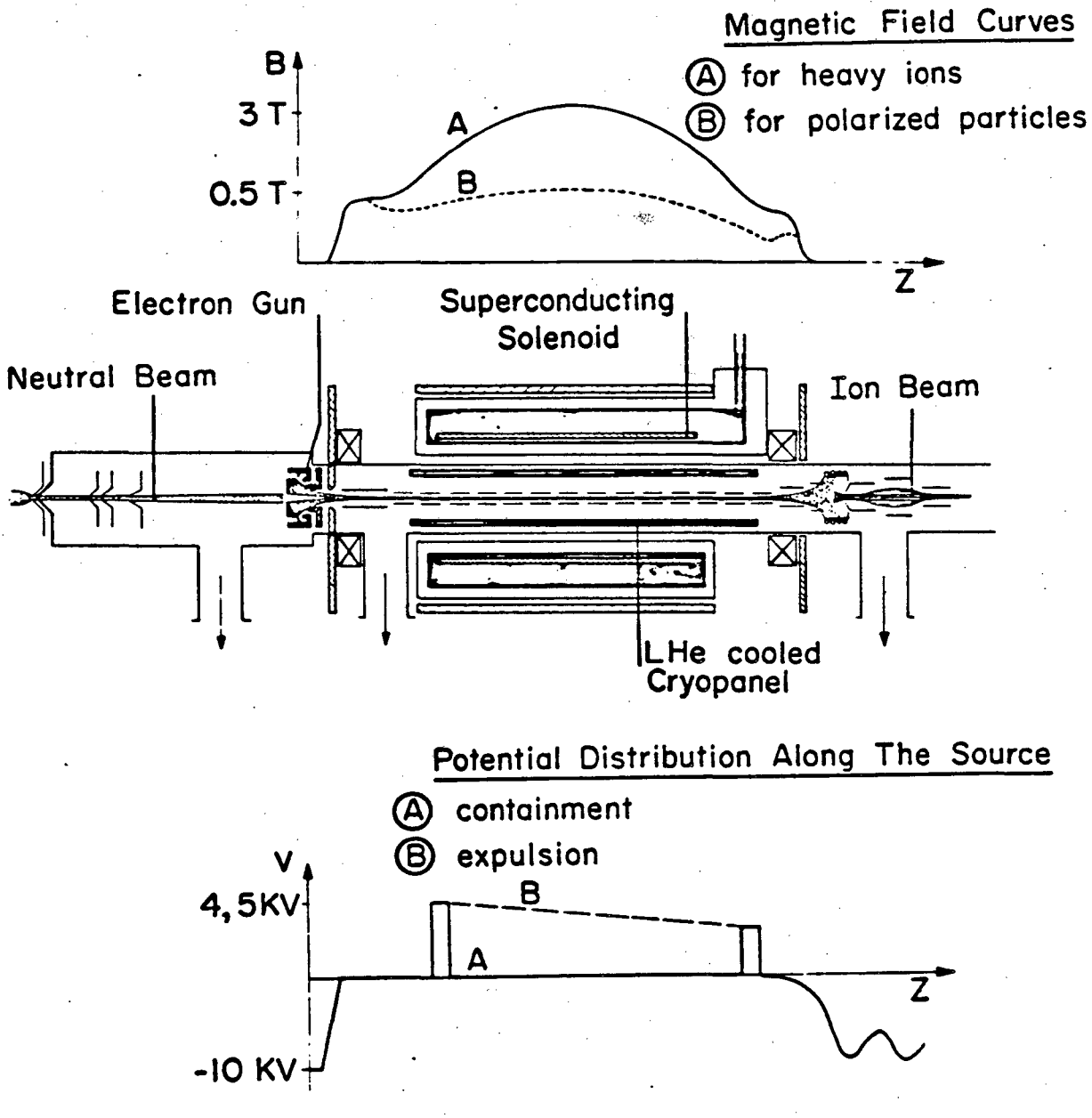

Figure 34.

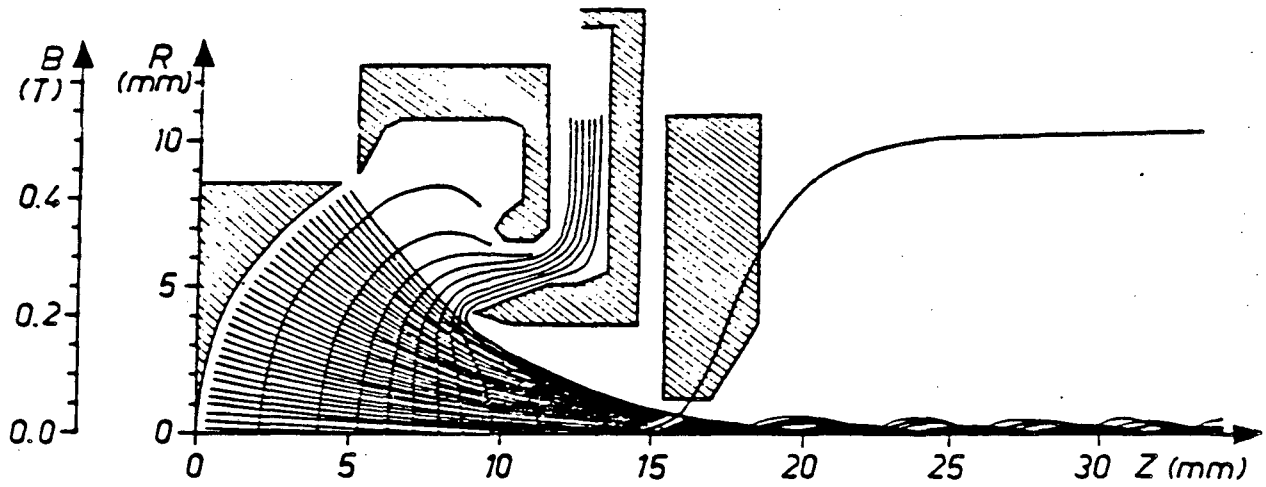

Figure 35.

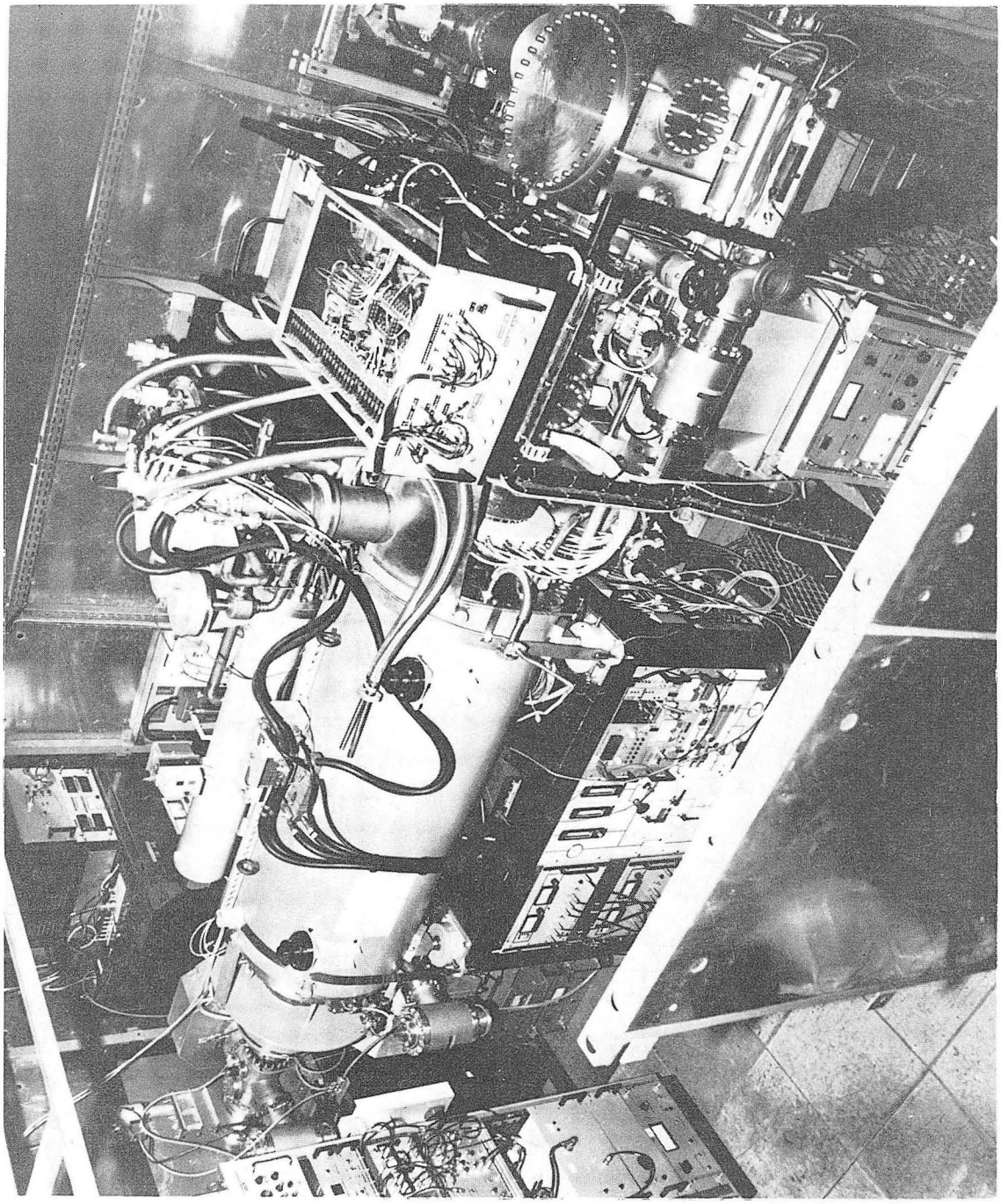

XBB 823-1791

Figure 36

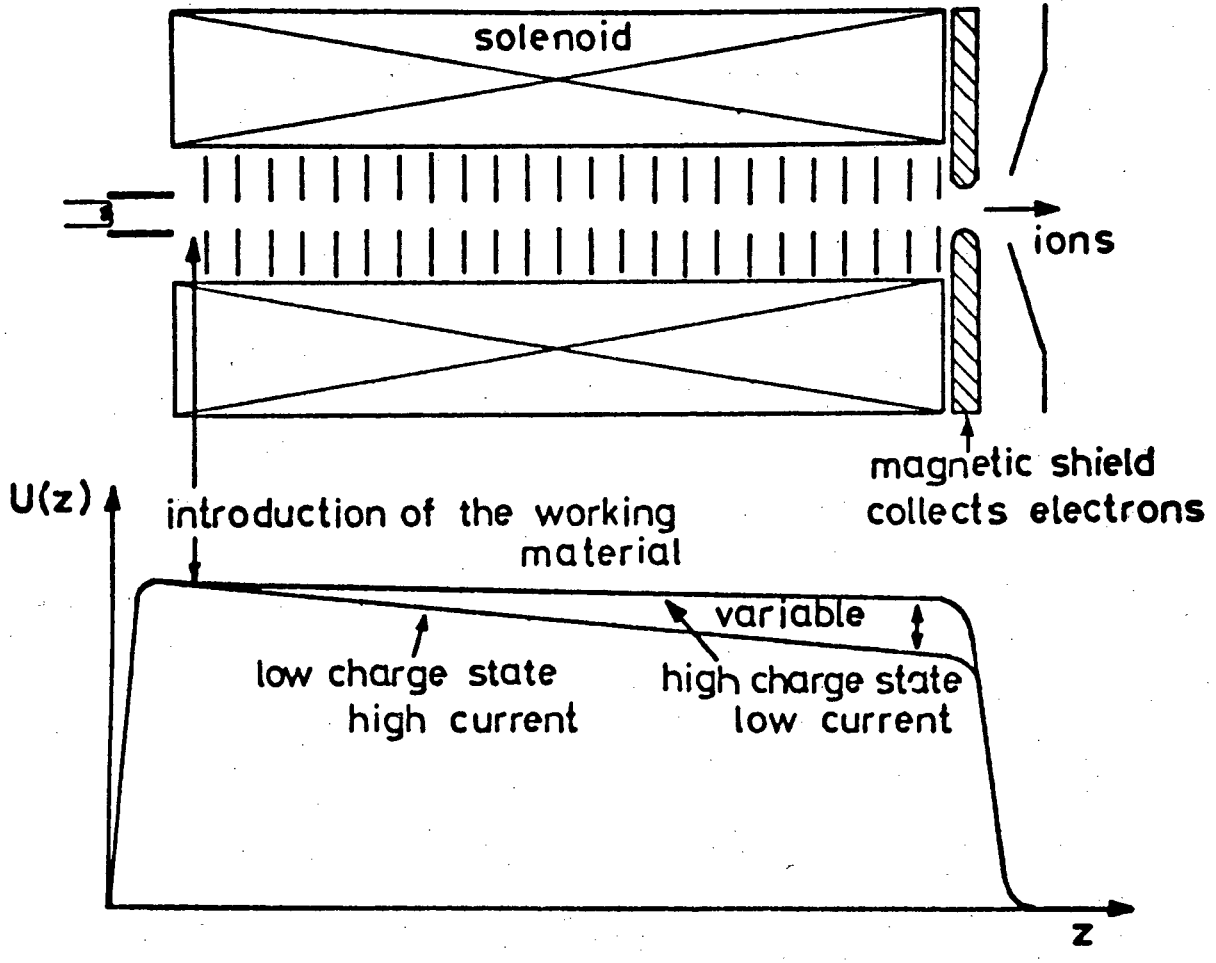

Figure 37.

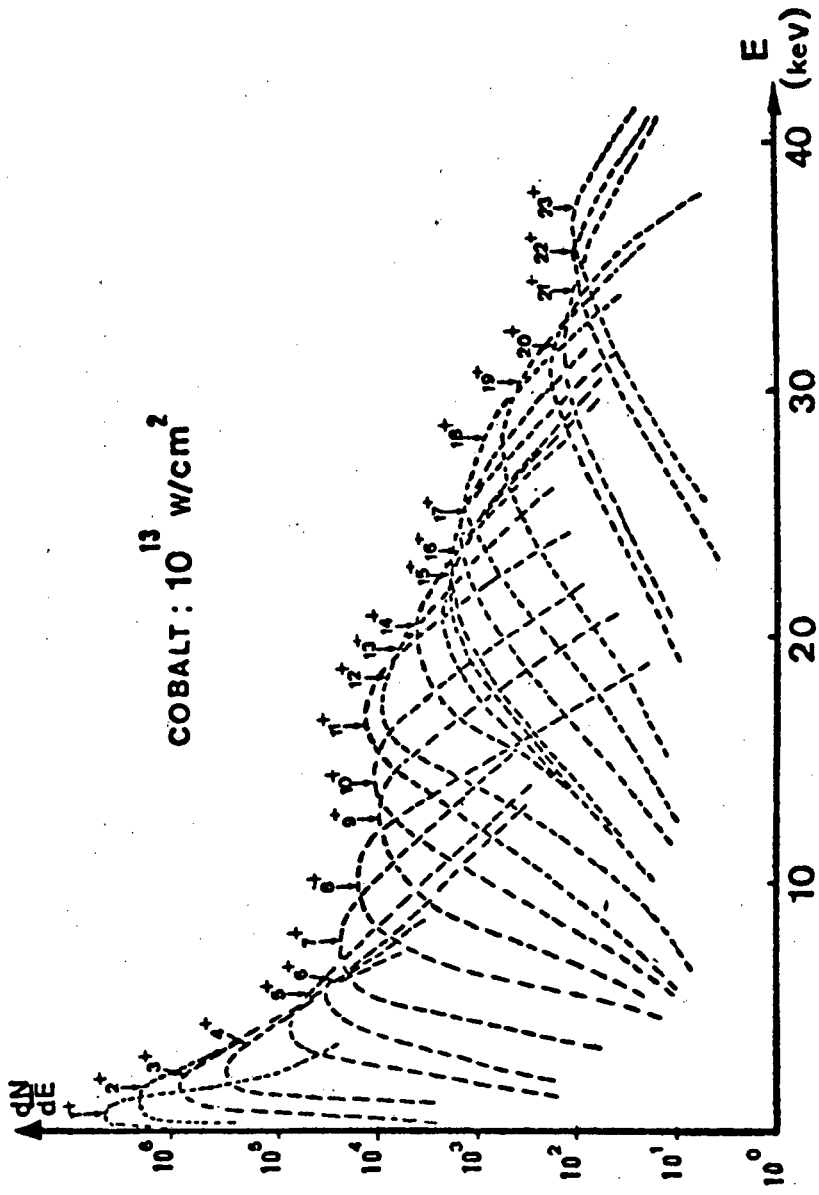

Figure 38.

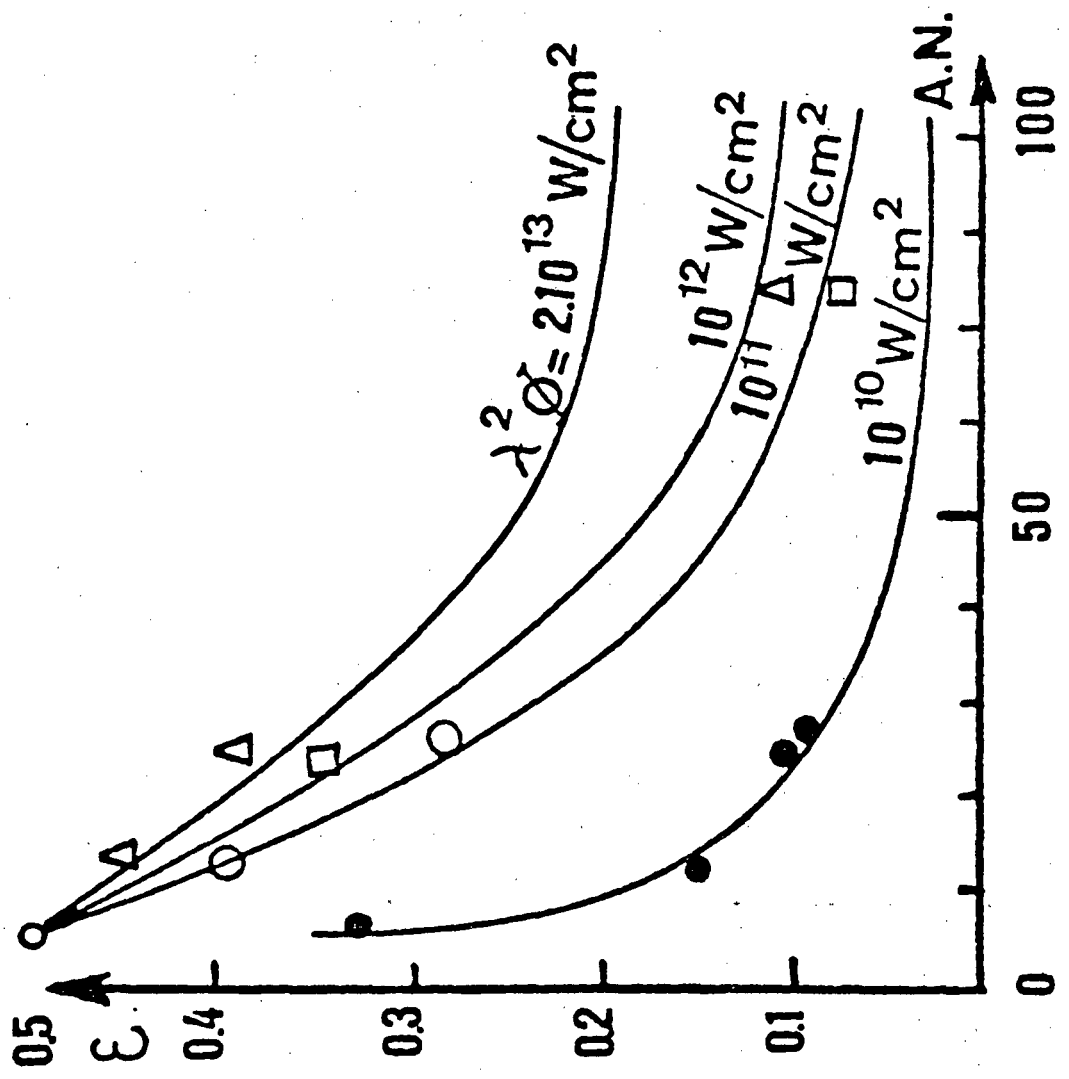

Figure 39.

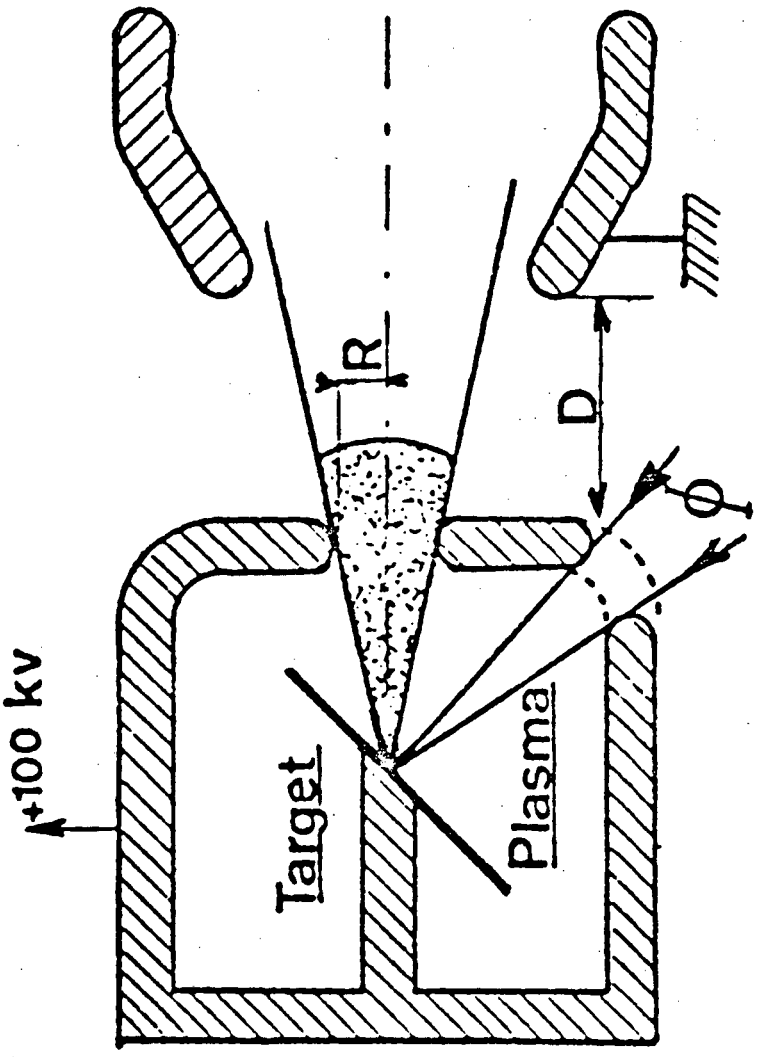

Figure 40.

TECHNICAL INFORMATION DEPARTMENT
LAWRENCE BERKELEY LABORATORY
UNIVERSITY OF CALIFORNIA
BERKELEY, CALIFORNIA 94720